Recent Advances in Transition Metal Phosphide Nanocatalysts for H_2 Evolution and CO_2 Reduction

Saman Shaheen, Syed Asim Ali, Umar Farooq Mir, Iqra Sadiq and Tokeer Ahmad *

Nanochemistry Laboratory, Department of Chemistry, Jamia Millia Islamia, New Delhi 110025, India;
samanshaheen@gmail.com (S.S.); syedasimali954@gmail.com (S.A.A.); umarmir310@gmail.com (U.F.M.);
iqrasadiq62@gmail.com (I.S.)
* Correspondence: tahmad3@jmi.ac.in; Tel.: +91-11-26981717 (ext. 3261)

Abstract: Green hydrogen energy has captivated researchers and is regarded as a feasible option for future energy-related aspirations. The emerging awareness of renewable energy-driven hydrogen generation and carbon dioxide reduction calls for the use of unconventional schematic tools in the fabrication of nanocatalyst systems. Transition metal phosphides are state-of-art, cost-effective, noble-metal-free materials that have been comprehensively examined for sustainable energy-driven applications. Recent reports on these advanced functional materials have cemented their candidature as high-performance catalytic systems for hydrogen production and for carbon dioxide conversion into value-added chemical feedstock. Bimetallic NiCoP (238.2 mmol g^{-1} h^{-1}) exhibits top-notch catalytic competence toward photocatalytic HER that reveals the energy-driven application of a pristine class of TMPs, whereas heterostructured Ni_2P/CdS was found to be fit for photochemical CO_2 reduction, as well as for HER. On the other hand, pristine Ni_2P was recently ascertained as an efficient electrocatalytic system for HER and CO_2RR applications. A wide array of physico-chemical modulations, such as compositional and structural engineering, defect generation, and facet control, have been used for improving the catalytic efficiency of transition metal phosphide nanostructures. In this review, we succinctly discuss the proficiency of transition metal phosphides in green hydrogen production and carbon dioxide conversion via photochemical and electrochemical pathways. We detail the significance of their structural properties and brief the readers about the synthetic advancements without deviating from our goal of summarizing the recent achievements in energy-driven applications.

Keywords: transition metal phosphides; CO_2 reduction; H_2 generation; photocatalysis; electrocatalysis

1. Introduction

The devastating effects of global warming and climate change have motivated researchers to focus their attention beyond fossil fuels and their various modified derivatives. The unchecked release of carbon dioxide (CO_2) has drastically perturbed the flora and fauna of Earth's ecosystems and has put several species on the verge of extinction, as well as threatened the adaptation of many others [1]. Annually, 32.8 billion tonnes of CO_2 are released into the atmosphere from the consumption of fossil fuel derivatives such as coal and petroleum [2]. According to the special report proposed by the International Energy Agency (IEA), it is anticipated that the global energy demand will rise by about 25% in the coming two decades because of population expansion, and the energy associated with CO_2 release will increase by about 35.8 megatons per year in 2040 [3]. These catastrophic predictions and current environmental maladies necessitate a paradigm shift to a sustainable energy solution. Various accords such as the Kyoto Protocol and the Paris Agreement have been signed to combat CO_2 release collectively at multiple levels [4]. The inherent heating nature of CO_2 has the potential to cause fluctuations in the seasonal patterns of El Nino and La Nina, which govern the nature of winds worldwide [5]. If standard protocols are

not implemented to control the unrestricted venting of CO_2, the atmosphere of our planet will be like that of Venus, and the planet will become a non-colonized gas chamber [6]. Consequently, the average global temperature and sea level will increase.

The development of any nation depends heavily on the manufacturing, automotive, and agriculture sectors, but all of these industries require efficient fuels for consequential output. Hence, the optimization of energy resources is economically fundamental for any nation to achieve an equilibrium between the demand and supply chains. Hydrogen (H_2), as a renewable energy resource, has various benefits such as remarkable gravimetric density and higher calorific value, which make it a viable alternative to fossil derivatives [7–10]. Currently, steam reforming of fossil fuels is the standard practice for the generation of bulk H_2. However, the nature of this type of H_2 is not at all eco-friendly and augments greenhouse gas emission. Therefore, green H_2 energy via overall water splitting is sought out as an environmentally benign way to extract H_2 [11]. Currently, the research community is committed to elevating the efficiency of the H_2 evolution reaction (HER) and CO_2 reduction reaction (CO_2RR) to the extent that they become a tandem antidote to the climatic concerns of the planet.

The development of HER and CO_2RR is hindered by the non-achievement of cost-effectiveness and efficiency in meeting large-scale operational endeavors. HER and the conversion of CO_2 into value-added chemicals such as hydrocarbon fuels via photochemical, electrochemical, and photo-electrochemical pathways offer a great deal of cost efficiency and production output because these green routes have been significantly scrutinized [12–16]. Nanocatalysis has proven to be an effective pathway to an environmentally benevolent protocol for CO_2 reduction and H_2 generation [17]. Nanostructures exhibit significantly higher exposed active sites, and because of quantum confinement effects, they possess optoelectronic properties that are superior to their bulk counterparts [18]. Therefore, exploiting nanocatalysts to carry out HER and CO_2RR is instrumental to a scalable production of H_2 and carbon-based value-added chemicals. There are numerous fabrication techniques that have been explored for designing the nanostructures of advanced functional materials, such as the reverse micellar system [19–22], the polymeric precursor route [23], the hydrothermal/solvothermal method [24], etc.

CO_2 is an ideal starting material for the production of energetic chemical fuels that are desired to meet energy requirements in the future [25]. Photochemical and electrochemical CO_2RR pathways are considered to be economical and environmentally benign routes for the conversion of CO_2 into valuable feedstocks such as CO, HCOOH, CH_4, C_2H_4, CH_3COCH_3, and CH_3OH, without producing any undesirable by-products [26–28]. The schematic representation of the photocatalytic conversion of CO_2 into valuable feedstock is demonstrated in Figure 1. In addition, there is a process of syngas (CO+H_2) generation via the photocatalytic/electrocatalytic reduction of CO_2 in an aqueous solution that is a vital intermediate for enhancing the yield of hydrocarbon fuels. The reverse water–gas shift reaction (RWGS) is a sustainable pathway of CO_2 conversion that has received recognition for its widespread application of CO_2 as the starting material [29]. However, all of these HER and CO_2RR routes demand Earth-abundant, advanced functional materials that can throttle secondary reactions such as the back recombination of charge carriers, the methanation reaction, or competing HER reactions in the case of CO_2 sequestration.

Various classes of materials have been explored as electrocatalysts and photocatalysts, including metals [30], metal alloys [31], metal oxides [32,33], metal sulfides [34], metalorganic frameworks (MOFs), transition metal chalcogenides [35,36], and carbon-based materials like graphene or carbon nanotubes [37,38]. However, metal oxides exhibit low conductivity, and metal sulfides are limited by their photo-corrosiveness. Transition metal phosphides (TMPs) have emerged as efficient catalysts with high electrical conductivity and exceptional physicochemical properties. The catalytic efficiency of TMPs is highly dominated by their intrinsic properties such as light absorptivity, the presence of active sites for the adsorption of reactive species, transportation capability, tunable band potential, and photosensitization. It is relatively difficult to obtain scalable energy-related performance via

pristine TMPs, so in order to achieve higher performance, various strategies have been formulated, such as synthetic modulations, cocatalyst incorporation, heterojunction formation, and compositional and morphological modifications. The fabrication of TMPs fundamentally hinges upon the metal-to-phosphorus ratio and the sources of phosphorus. Therefore, researchers are trying to optimize the synthetic methodologies of TMPs that elute non-toxic or less harmful by-products and that are environment friendly in nature. Although TMPs exhibit higher catalytic response for HER and CO_2RR applications, there are still several bottlenecks that need to be rectified prior to their large-scale commercial application.
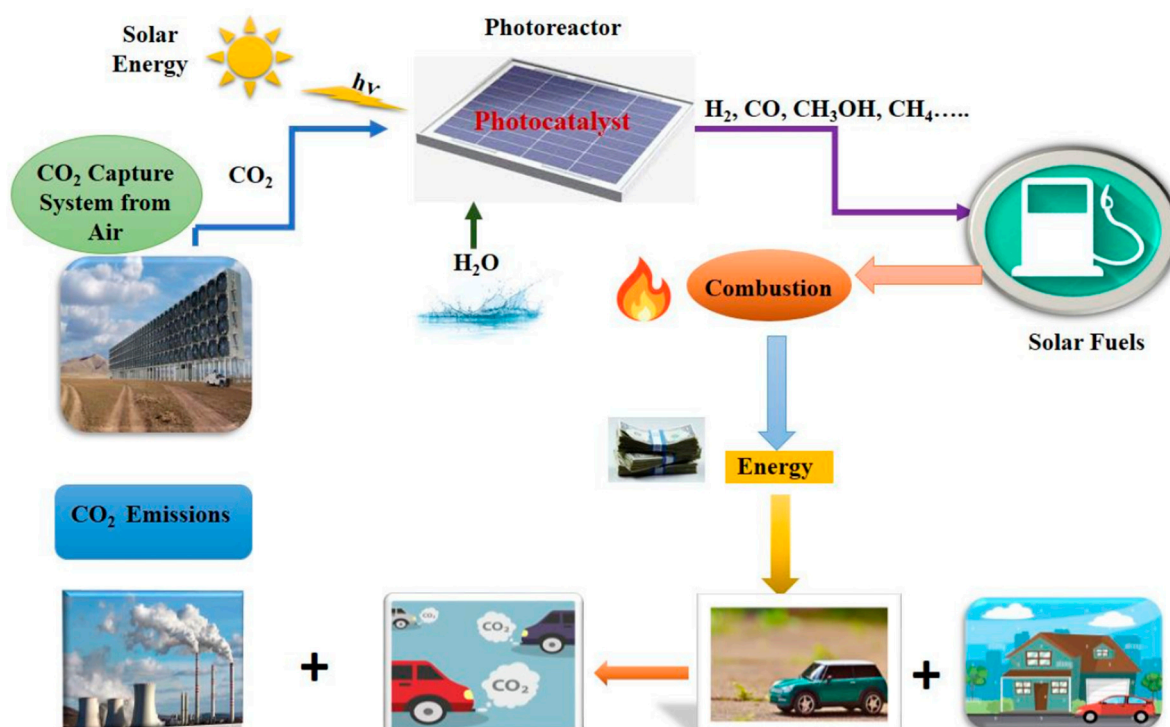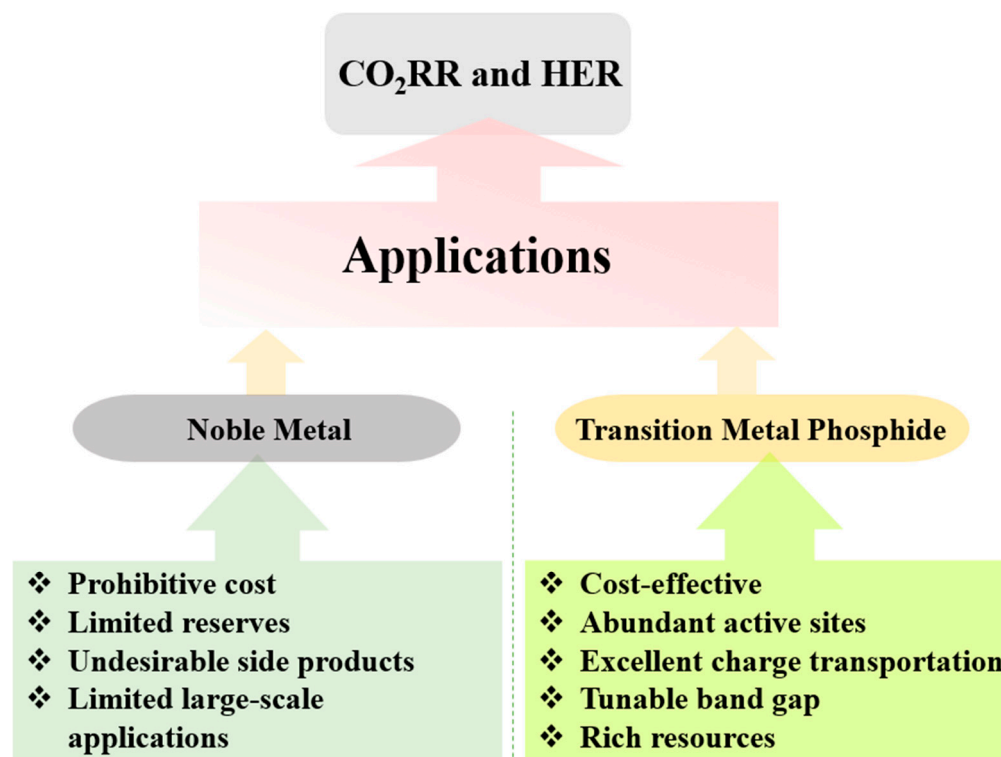

Figure 1. Schematic demonstration of photocatalytic reduction/conversion of CO_2 into solar fuel. [Reprinted with permission from Ref. [1]. Copyright 2023, John Wiley and Sons].

TMPs are an emerging class of advanced materials believed to be potent candidates that can replace precious noble metal-based catalysts [39]. The role of TMPs in nanocatalysis is not only limited to direct utilization. Instead, they can also be employed as cocatalysts. In the last few decades, it has been observed that cocatalyst loading is one of the best ways to enhance photochemical and electrochemical efficiencies by improving their light-harvesting, electrical conductivity, and physicochemical properties through interface engineering, alongside providing multifunctional active sites for surface adsorption [40,41]. Both the activity and selectivity of HER and CO_2RR can be enhanced by using cocatalysts. Among different types of cocatalysts, noble metals such as Pt, Pd, Au, Ag, and Ru have been comprehensively studied for the photocatalysis of HER and CO_2RR [42–45]. However, due to their scarcity and the whopping cost involved, their large-scale applicability is limited. An advanced, economical, and efficient method is the need of the hour. Therefore, developing non-noble-metal-based cocatalysts which fulfil the requirement of being cost-effective is requisite. Among various non-noble-metal-based cocatalysts, TMPs are classified as promising candidates for photocatalysis and electrocatalysis. Antil et al. [44] fabricated novel NiCoP@ZnCo-MOF photocatalysts and displayed an augmented rate of H_2 (8583.4 $\mu mol\ g^{-1}\ h^{-1}$). The group conducted comparative analysis between as-synthesized TMP nanocatalysts relative to the noble-metal-based catalytic system of Pt@ZnCo-MOF (8885.7 $\mu mol\ g^{-1}\ h^{-1}$). The rate of H_2 production of the TMP-based photocatalyst was found to be nearly analogous to its noble metal counterpart. Thus, we can corroborate

TMPs as a viable substitute for noble metals in assisted catalysis for advanced HER applications. An illustrated diagrammatical comparison is provided in Figure 2 for the better selectivity of TMPs over noble metal catalysts.

Figure 2. Diagrammatic illustration of CO_2RR and HER with respect to noble metal and transition metal phosphide.

The schematic landscape of TMPs synthesis, properties, and energy-driven applications such as energy conversion and energy storage are illustrated in Figure 3. In 2005, for the very first time, Liu et al. [46] predicted the catalytic excellence of Ni_2P by considering density functional theory and evaluating its photocatalytic activity towards HER. The scope of the CoP cocatalyst has been analyzed to augment the photocatalytic efficiency of two-dimensional g-C_3N_4. In the CoP/g-C_3N_4 heterostructured catalyst, photo-generated electron transference occurs from g-C_3N_4 to the surface of CoP active sites in light [46,47]. The surface electrons react with the absorbed protons, resulting in the supplication of photocatalytic HER activity. Recent reports have also proven the potential of other nickel-based TMPs such as Ni_2P, $Ni_{12}P_5$, and Ni_3P for enhancing the light absorption capacity of g-C_3N_4, due to which they are believed to possess high photocatalytic activity in HER [48]. TMPs have achieved superior photocatalytic HER and CO_2RR activities, as revealed by the literature review [49]. Hence, researchers need to focus on the developments in the field of TMP-assisted nanocatalysis. This review summarizes the recent advances in TMPs towards HER and CO_2RR applications.

Figure 3. Schematic landscape of TMPs synthesis, properties, and energy driven applications.

2. TMPs Structure and Its Significance

TMPs are versatile catalysts that consist of transition metals bonded with phosphorus (P) atoms. The structure of TMPs is of great significance and can vary depending on the types of metals, the number of P atoms, and the bonding interactions between them. TMPs possess different structures and morphology depending on the other metals and their interactions with the P atoms [50]. In addition, factors like the reactant precursors of transition metal and P, stoichiometry, and synthesis conditions also govern the structural properties of TMPs [51]. In TMPs, the P atom enters the lattice structure of transition metals to form interstitial compounds that act as efficient catalysts for energy conversion processes [52]. The structural modifications on introducing the P atom in the lattice structure of transition metal (M) is an elongation in the bond length of the M-P bond, which results in decreased interactions of M-M bonds and the compression of d-bands [53]. This lattice mismatch tunes the Fermi levels of M, favoring their electronic conductivity and mass diffusion characteristics [54]. TMPs exhibit unique crystal structure where the M atoms form the trigonal prismatic structure, in which the interstitial voids are occupied by P atoms in the smallest structural unit. In contrast, the excess metal ions form nine-fold tetrakaidecahedral structures [55], as represented in Figure 4a,b. The P atom can interact with the transition metal lattice. These structural units can cooperate and have the ability to form miscellaneous lattice types. Variations in the M/P ratio significantly affect the lattice structure of TMPs. Thus, this ratio also controls the catalytic efficiency of TMP nanocatalysts. In a TMP structure, P exhibits relatively higher electronegativity, attributed to the fact it accepts protons readily. This structural feature of TMPs boosts their catalytic action towards HER and CO_2RR as facilitated H^+/CO_2 surface adsorption takes place quickly due to higher electronegativity of P atoms [50]. Therefore, the P content in TMPs is central to determining their catalytic activity. Based on that, they can be classified as transition-metal-rich TMPs (M-rich TMPs) or P-atom-rich TMPs (P-rich TMPs), depending on the M/P ratio [56]. In M-rich TMPs, the M/P ratio is comparatively higher, due to which M–M interactions profoundly affect the physiochemical properties of TMPs. These compounds often exhibit a lower P content than stoichiometric or P-rich TMPs [57]. The excess of M atoms results in unique properties and structures of TMPs. M-rich TMPs are commonly synthesized under high-temperature conditions, such as through the reaction of metal precursors with P sources. However, P-rich TMPs hold a relatively higher ratio of P to transition metal. These compounds have excess P and exhibit unique properties based on their high P content. The crystal structure of P-rich TMPs is depicted in Figure 5a–f below [56]. M-rich TMPs

exhibit metallic properties, whereas P-rich TMPs show semiconducting behavior. The metallic behavior in M-rich TMPs is familiar with that of noble metals, showing excellent conducting properties [42]. P-rich TMPs are often synthesized through reactions that involve the addition of excess P or P-rich precursors. For instance, M-rich TMPs bestow higher conductivity and stability than P-rich TMPs due to the larger M–M and M–P bonds than non-conductive P–P bonds.
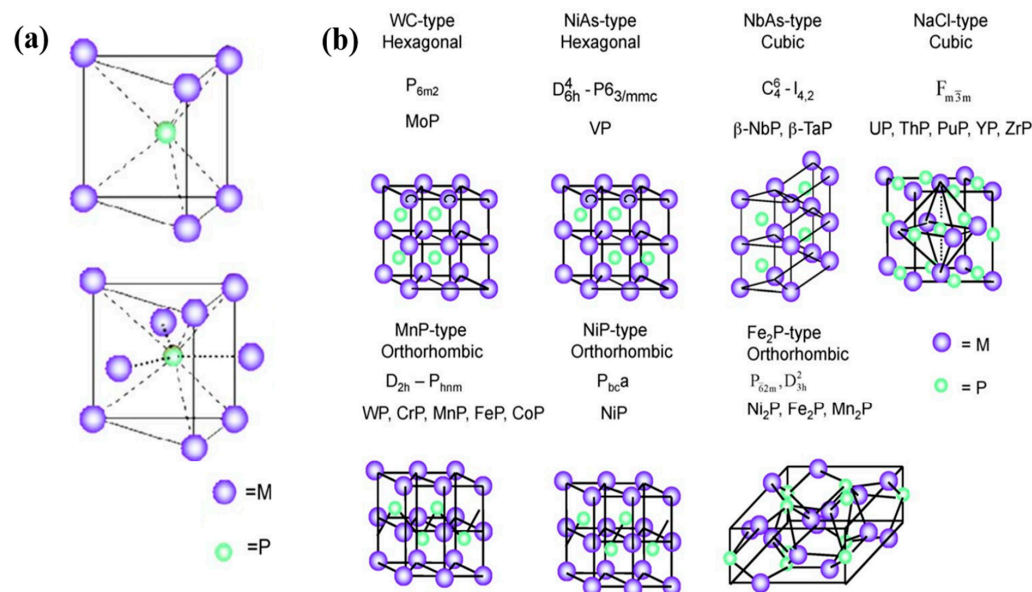

Figure 4. (**a**) Triangular prism and tetrakaidecahedral structures in phosphides and (**b**) crystal structures of metal-rich phosphides. [Reprinted with permission from Ref. [55]. Copyright 2009, Catalysis].
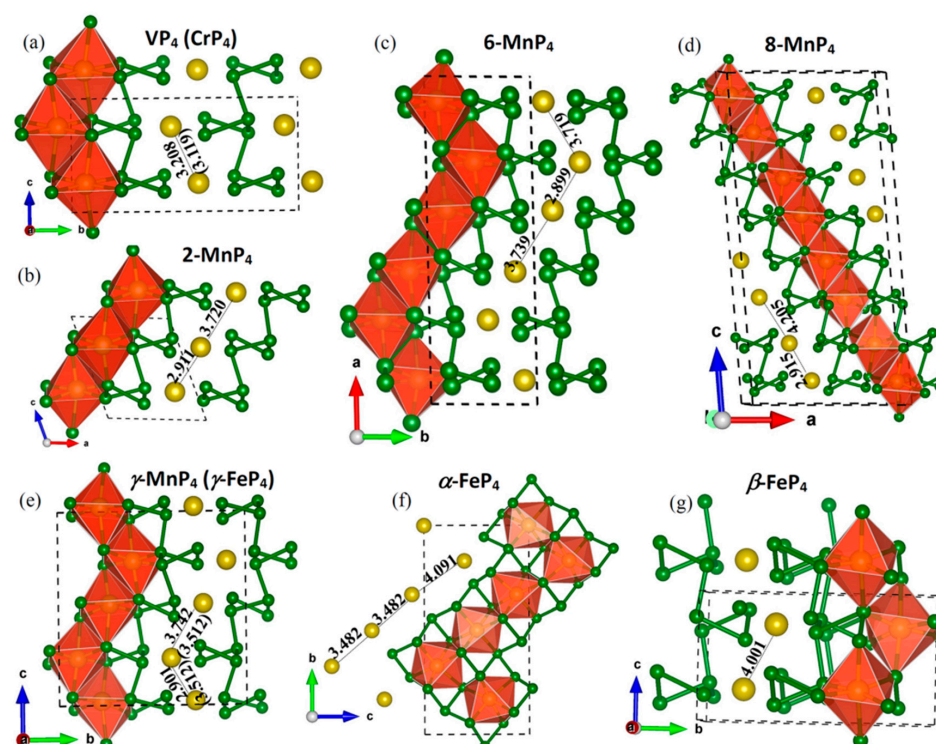

Figure 5. Crystal structures of 3D-TMP$_4$ (TM = V, Cr, Mn, and Fe) polyhedron view. The TM and P atoms are represented as big yellow spheres and small green spheres, respectively. [Reprinted with permission from Ref. [56]. Copyright 2018, American Chemical Society].

3. Structural Significance

The structural ascendency of TMPs, due to the introduction of P-atoms in the lattices of transition metal ions, dramatically affects the optoelectronic properties of these interstitial materials, thus making them excellent HER and CO_2RR catalysts [58–60]. Incorporated P atoms moderately tune the interspace between the transition metal atoms that restricts their molecular interaction. It leads to the shrinking of d bands and increasing the concentration of energy levels in the vicinity of the Fermi center [61]. This excellent optoelectronic modulation in TMPs escalates their catalytic efficiency of the order of noble-metal based catalytic systems [62,63]. The structural engineering of TMPs is one of the finest strategic tools to ameliorate their performance towards HER and CO_2RR applications. Recent reports of TMPs support the fact that developing heterojunctions, hollow and nanoarray structures, significantly enhance their scope of applicability. Heterojunction formation allows for the interfacial charge transfer during photochemical HER and CO_2RR, which effectively subdues the back recombination reactions and assures the utilization of active electron carriers in primary reduction reactions. On the other hand, the formation of hollow structures eases the adsorption pathways of reactant species by providing higher exposed active sites available for surface reactions and sufficient mass diffusion routes [64–68]. Higher surface areas and surface roughnesses in nanoarrays facilitate the contact compass between catalytic system and adsorbed species. The structural properties of TMPs are pretty significant in modulating their electronic properties, leading to remarkable catalytic responses in energy-related applications. Other than structural engineering, tuning the physicochemical properties of TMPs also hinges on their compositional and morphological properties.

4. Advances in TMP Fabrication

For the comprehensive exploitation of TMPs, optimizing synthetic routes is essential to achieve cost-effectiveness and environmental friendliness. Conventional methods used to fabricate TMPs, such as temperature-programed reduction under H_2 atmosphere or the ball milling method, are restricted to the synthesis of bulk TMPs only. However, for constructing nano-dimensional TMPs, fabrication routes can be classified on the basis of P sources used and the different methods involved. Synthetic pathways have been classified based on P sources such as organic phosphines (trioctylphosphine), hypophosphites ($NH_4H_2PO_2$, NaH_2PO_2), elemental phosphorus (white, red), and phosphorenes [13]. Phosphorenes are the exfoliated monolayers of black P that have also been utilized as P precursors for TMP engineering [69]. One different approach to designing TMPs is the pyrolysis of P and carbon-based precursors alongside the source of the transition metal ion. Integrating carbon-based materials during TMP synthesis impedes the agglomeration of TMP nanoparticles and accelerates their conductivity. Therefore, different morphologies and particle sizes can be achieved based on the use of varying P sources for TMP nanostructures. The discrete synthesis method for designing TMPs can vary metal to metal or depending on the desired morphology, the targeted energy-related application, and the chosen precursors of P [70]. Researchers often optimize the reaction conditions and other parameters such as reducing the agent and solvent system to obtain the desired physicochemical properties and morphology of the prepared TMP nanocatalysts [71]. Synthesizing TMP nanostructures typically involves diverse physical and chemical routes such as solid-state reactions [72], the phosphorization of metal precursors [73–76], chemical vapor deposition (CVD) [77], and hydrothermal pathways [78–82].

In the usual practice, the solid-state method proceeds via heating a mixture of transition metal precursors (metallic powder or metal oxides) alongside a P source at significantly higher temperatures under an inertial atmosphere to subdue any undesired defects or oxide impurities [72]. The reaction advances through a series of intermediate steps that lead to the development of the desired TMP nanostructures. As its name suggests, the phosphorization of metal precursors comprises the precursor of the desired metal and is minted with the source of P, such as red or white phosphorus. The phosphorization reaction can occur either in solution or in the gas phase, depending on the nature of transition metal precursor and

P source. The obtained reaction mixture is then further processed to isolate the pristine TMPs without any foreign impurities. The CVD technique is generally utilized to deposit thin films or coatings of TMPs. In this pathway, relatively volatile metallic precursor is integrated with the P-containing precursor, and the resulting mixture is introduced into the reaction chamber, followed by that reactant mixture decomposed at high temperatures leading to the deposition of the TMPs onto a substrate. The hydrothermal/solvothermal route is an environmentally benign chemical route that offers great deal of output and control over morphology for far-reaching applications of TMP nanostructures [80]. It involves the reaction of metal precursors with the P source in generally aqueous media and sometimes in other solvents under high-pressure and high-temperature conditions. The organic solvent environment is developed in the reaction media to achieve the desired morphology. The reaction is typically carried out in an autoclave, where the reaction mixture is subjected to the particular reaction conditions. The main advantage of procuring this route is the formation of well-defined TMP nanoparticles. Considering the aforementioned synthetic routes of TMPs, we manifest that all these pathways have their respective advantages and disadvantages. However, in our vision, the hydrothermal route has far-reaching applications for the sake of energy-related operations of TMP-based hybrid materials.

5. TMP Photocatalysts for HER and CO_2RR Applications

Over the past few years, the optoelectronic properties and chemical stability of TMPs have made them promising catalytic systems for photochemical HER and CO_2RR applications. TMPs such as FeP [83], CoP [84], NiCoP [85], MoP [86], and Cu_3P [87] have been investigated in the field of nanocatalysis and are known to display exceptional activity and selectivity towards HER and CO_2RR applications. There are various methods of enhancing the photocatalytic performances of TMPs such as metallic/non-metallic doping [88], surface modulation [89], and mixing with other nanomaterials to form heterojunctions [90]. For instance, the integration of noble metals like Au and Pt with TMPs ameliorates their photocatalytic activity towards HER and CO_2RR [49,91]. In the past few decades, much of the attention has been placed on improving the efficiency of photocatalytic processes by developing and probing miscellaneous catalytic systems. Therefore, to achieve this goal, researchers are persistently trying to enhance the activity and selectivity of TMP-based photocatalysts. However, this transformation is limited by the quick recombination rate of photogenerated electron–hole pairs and the restricted photo-sensitization of light absorbers during photocatalytic operations. These two obstacles are the major bottlenecks of photocatalytic HER and CO_2RR operations that impede their quantum efficiency in achieving H_2 and carbonaceous value-added chemicals [49]. The tailored band energy of TMP nanocatalysts allows an accelerated harvesting of light that ultimately leads to the flow of uninterrupted photo-induced charge carriers, allowing longer runs of photocatalysis. The prevention of the back recombination of photo-generated electron–hole pairs can be successfully achieved by developing appropriate cocatalysts that would generate suitable interfaces, such as Schottky junctions, S-schemes, Z-schemes, p-n heterojunctions, and type II heterojunctions, leading to the fast movement of charge carriers from one component to the other, thus reducing the probability of electron–hole pair recombination [92–94]. Although, some secondary side reactions result in the photocatalytic CO_2RR. HER is one of the competent reactions in the conversion of CO_2 to CO. Therefore, the recent trends of TMP-assisted photocatalytic applications have imbibed these limiting factors, as demonstrated by the reports of TMPs discussed hereafter in this section.

Li et al. [78] fabricated a Ni_2P/$ZnIn_2S_4$ heterostructure to examine its scope towards photocatalytic water splitting. Optimized Ni_2P/$ZnIn_2S_4$ heterojunctions exhibited a remarkable H_2 evolution rate of ~2.1 mmol g^{-1} h^{-1}, which can be attributed to the better synergism between the photocatalytic components, the enhanced charge separability, the larger surface area, and the outstanding electron transport ability. Shen et al. [95] synthesized EosinY-Cu_3P-CNT (carbon nanotubes). The group reported an exceptional H_2 evolution rate of 17.22 mmol g^{-1} h^{-1}, which is owed to the efficient separation of charge

carriers in Eosin Y and enhanced electron transfer ability that symbiotically boosted the rate of H_2 generation in the TMP-based photocatalyst. Meng et al. [40] fabricated Ru-CoP-1:8/GCN (g-C_3N_4) photocatalysts via the wet chemical reduction method for efficient H_2 production. The reported study showed an exceptional rate of 1172.5 μmol g^{-1} h^{-1}. This report outlines the cost-effectiveness of Ru-CoP heterostructured catalytic system as compared to noble metal catalysts for photocatalytic applications. Gong et al. [86] developed Ni-MoP@NP$_{PF}$ (porous nitrogen-doped carbon nanofibers) via electrospinning followed by phosphorization as well as carbonization and showed the rate of CO production to be 953.53 μmol g^{-1} h^{-1}. It exhibited an impressive selectivity for CO of 98.95% due to the formation of Ni-N bonds. The mechanism proposed that the transfer of electrons occurs across the interface between the two catalysts, enhancing the rate of CO_2 reduction, as represented in Figure 6a. The photocatalyst revealed exceptional activity and selectivity for CO_2 reduction with Ni, as without Ni co-catalyst, the yield was found to be relatively inferior, as depicted in Figure 6b. The product selectivity of Ni-MoP@NC$_{PF}$ is realized by higher CO generation, as the optimized Ni-MoP@NC$_{PF}$ catalytic system exhibited greatly enhanced photocatalytic CO_2 reduction performance towards CO generation compared to CH_4 and H_2 product formation, as depicted in Figure 6c. Ni-MoP@NC$_{PF}$ provided channels for CO_2 diffusion and electron transport. This type of TMP-based catalytic system is the epitome of collaborative morphological, compositional, and hetero-interfacial engineering, as the distribution of Ni throughout the MoP@NC$_{PF}$ improved the transformation of CO_2 to CO. The main factors that regulate the degree of photocatalytic HER and CO_2RR processes are the separation, transfer, and recombination of electron–hole pairs. The photocatalytic activity of CO_2 conversion is ameliorated by the higher separation rate of photo-induced charge carriers or lower recombination rate ascribed to more electrons available for primary reduction reactions at the conduction band of TMP-based photocatalysts.
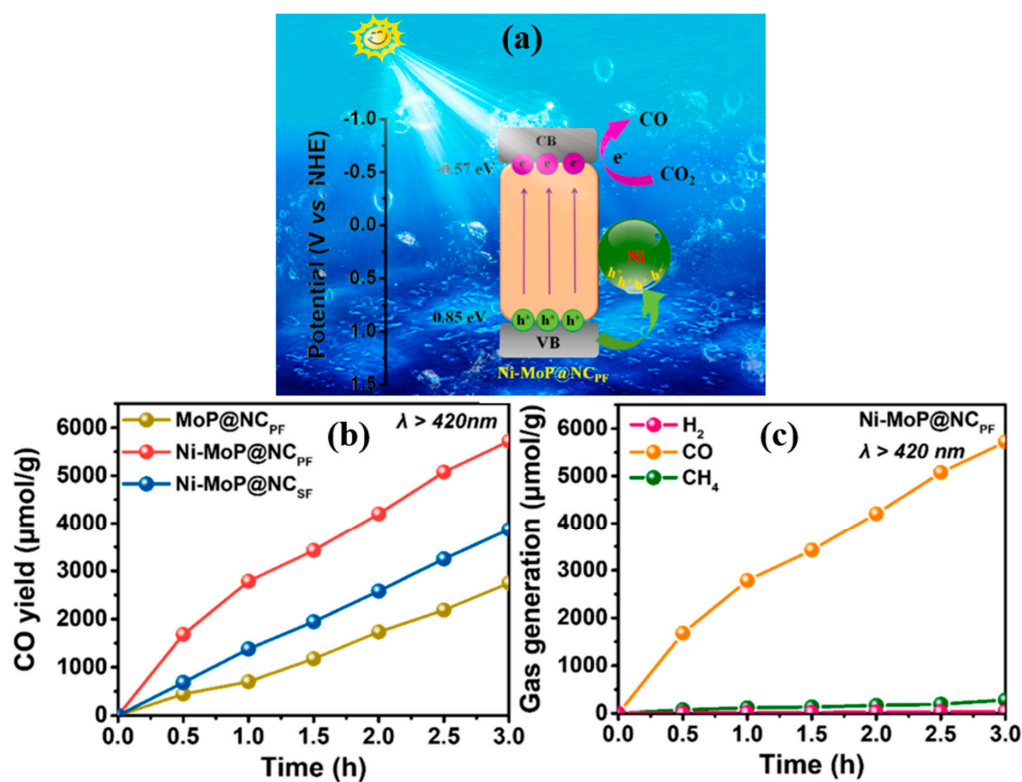

Figure 6. (**a**) The mechanism of Ni-MoP@NCPF as a photocatalyst for CO_2 reduction, (**b**) CO generation on various photocatalysts under visible light irradiation (with a UVCUT-420 nm filter) for 3 h, and (**c**) gas products of CO_2 reduction on Ni-MoP@NC$_{PF}$ under visible light irradiation for 3 h. [Reprinted with permission from Ref. [86]. Copyright 2022, Elsevier].

Sun et al. [79] fabricated Cu_3P-Ni_2P/g-C_3N_4 nanocatalysts via a solvothermal pathway to determine their photochemical HER efficiency. The H_2 production rate was found to be considerably efficient due to the formation of p-n heterojunctions, assisting in the facile charge transfer and exposure of a greater number of active sites. Figure 7a,b contain mechanistic sketches of Cu_3P-Ni_2P/g-C_3N_4-assisted photocatalytic H_2 generation and the transfer of electrons via heterojunctions after the advent of an internal electric field before and after visible light irradiation, respectively. Song et al. [96] fabricated WP-NC (nitrogen-doped carbon)/g-C_3N_4 heterojunctions for efficient H_2 generation via photocatalytic and electrocatalytic pathways. The optimized WP-NC/g-C_3N_4 catalyst exhibited an H_2 evolution rate as high as 1.2 mmol g^{-1} h^{-1}, owing to the deposition of NC layers over WP, which ameliorated the charge separation and transfer efficiency during photocatalytic water splitting.
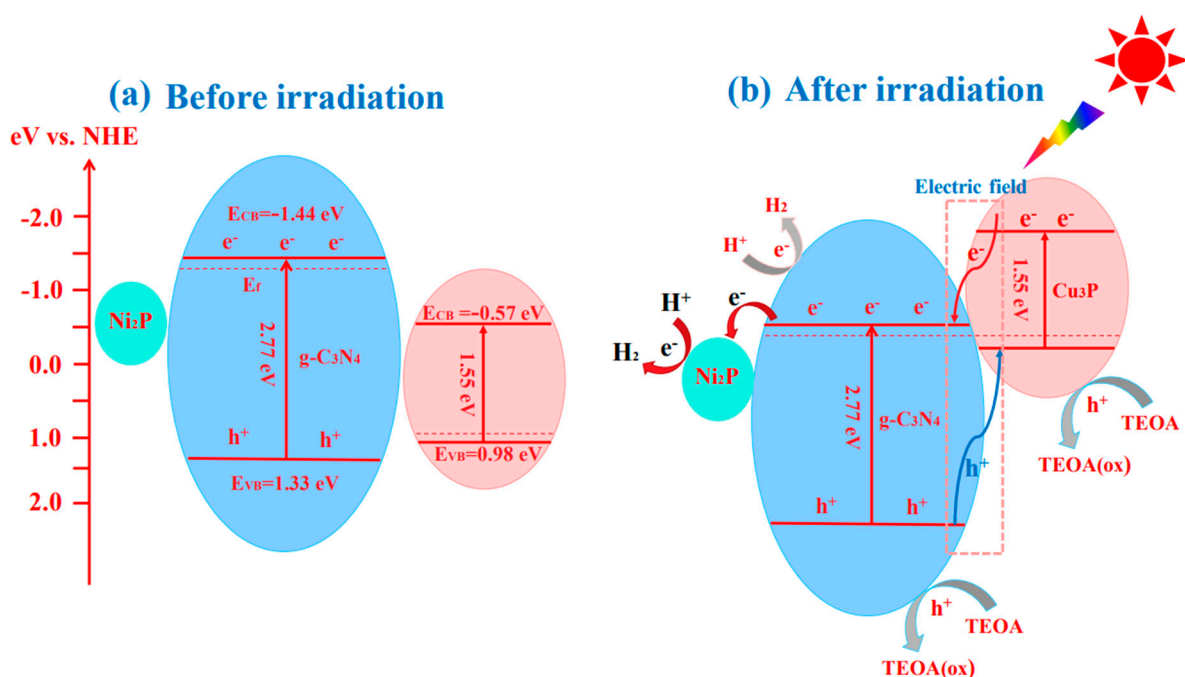

Figure 7. Mechanism of photocatalytic H_2 production for Cu_3P-Ni_2P/g-C_3N_4. [Reprinted with permission from Ref. [79]. Copyright 2020, John Wiley and Sons].

Su et al. [80] engineered Ni_2P/CdS photocatalysts via the hydrothermal pathway and studied their efficiency for HER and CO_2RR applications. The resultant band gap of the Ni_2P/CdS photocatalyst was found to be 2.16 eV with multiple production rate of H_2, CO, and CH_4 generation with porous and non-porous nanocomposites, as depicted in Figure 8. In this report, heterojunction formation played an essential role in the enhanced photocatalytic efficiency of Ni_2P/CdS, ascribed to the facilitated charge transfer. Guo et al. [83] synthesized an FeP/CN photocatalyst via the thermal decomposition method and reported the maximum rate of CO production to be 5.19 µmol g^{-1} h^{-1}. The synthesized catalysts exhibited the tremendous conversion efficiency of CO_2 to CO because of the greater active sites and facile charge transfer during the photocatalytic CO_2RR. Wang et al. [97] designed and synthesized novel Fe-doped CoP for CO_2 reduction to CO. The results reported a maximum selectivity of 90.3% (CO), and the rate of evolution was estimated to be 21 µmol h^{-1}. Fe doping assisted in subduing the activation energy barrier for intermediate formation and promoted CO evolution. Lv et al. [98] synthesized ultrathin NiCoP nanosheets to achieve an effective rate of HER (238.2 mmol g^{-1} h^{-1}). The reported bimetallic catalysts exhibited bifunctional properties such as electrocatalysis and photocatalysis efficiently. Duo et al. [99] designed FeP/CdS heterostructured photocatalysts via the solvothermal route, and the as-prepared nanocatalyst produced H_2 at the rate of 37.92 mmol g^{-1} h^{-1}.

This excellent HER was attributed to the charge separation and better electron transportation demonstrated by the heterojunction formation between the FeP and CdS. Li et al. [72] fabricated $Ni_2P/NiO/CN$ (graphitic carbon nitride) via solid–gas reaction for the conversion of CO_2 to CO and CH_4. The enhanced activity resulted from the formation of a p-n heterojunction between NiO and CN, while Ni_2P governed the activation and adsorption of CO_2 reactant species. The catalytic proficiency of TMPs towards photochemical HER and CO_2RR applications are tabulated in Table 1.
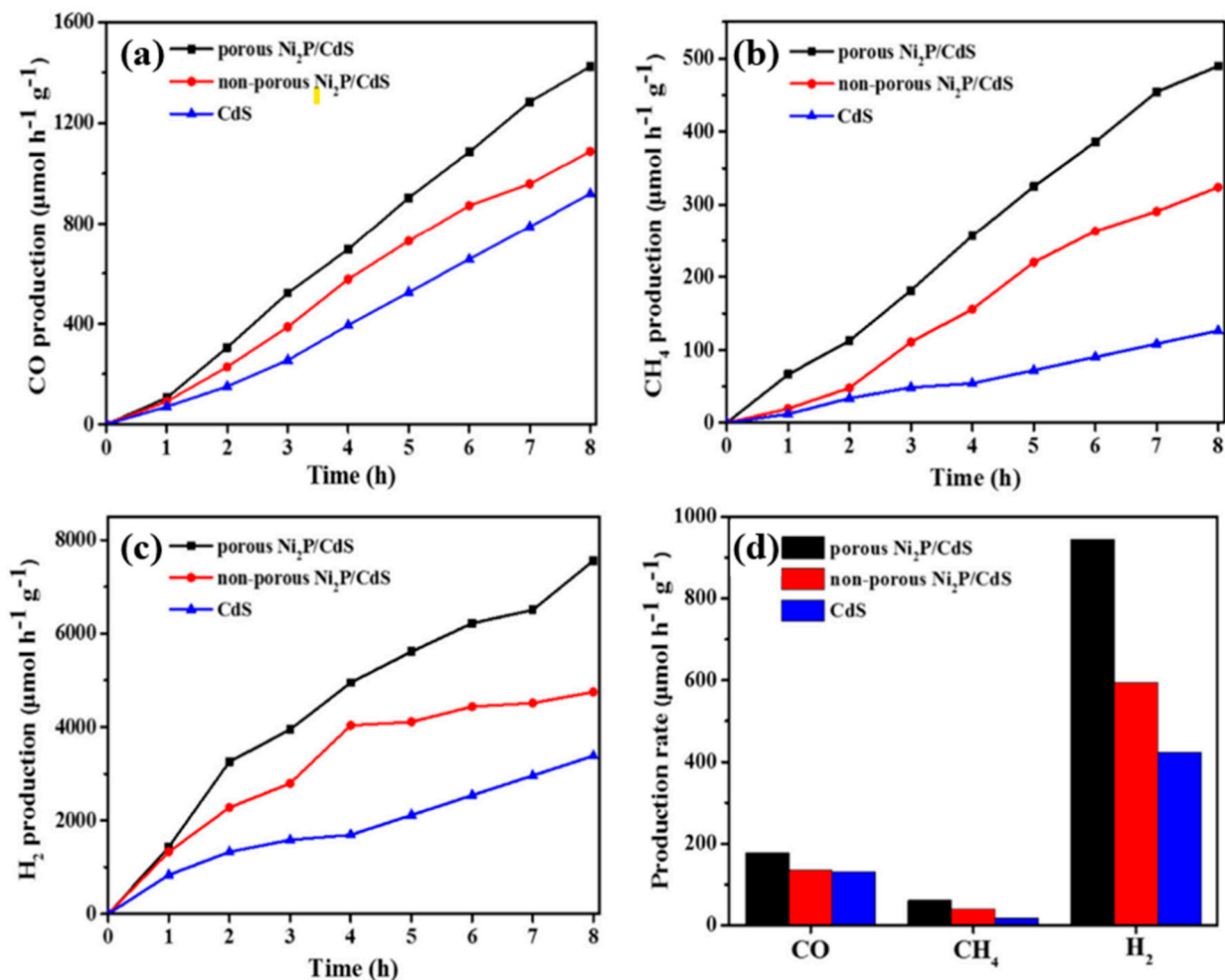

Figure 8. Photocatalytic rates of CO_2 reduction over porous and non-porous Ni_2P/CdS composites: (**a**) CO, (**b**) CH_4, (**c**) H_2, (**d**) survey of various gases. [Reprinted with permission from Ref. [80]. Copyright 2023, Elsevier].

Table 1. Transition metal-phosphide-based photocatalysts for HER and CO_2RR applications.

Catalysts	Synthesis Method	Application	Band Gap (eV)	Rate of HER/CO_2RR	Ref.
Ru-CoP-1:8/GCN	Chemical reduction	HER	2.25	1172.5 $\mu mol\ g^{-1}\ h^{-1}$	[40]
$Ni_2P/NiO/CN$	In situ gas–solid reaction	CO_2RR	2.6	CO (1.506 $\mu mol g^{-1}\ h^{-1}$) CH_4 (0.29 $\mu mol g^{-1}\ h^{-1}$)	[72]
$Ni_2P/ZnIn_2S_4$	Hydrothermal	HER	~2	2066 $\mu mol\ g^{-1}\ h^{-1}$	[78]
Cu_3P-Ni_2P/g-C_3N_4	Solvothermal	HER	2.7	6529.8 $\mu mol\ g^{-1}\ h^{-1}$	[79]
Ni_2P/CdS	Hydrothermal	HER and CO_2RR	2.16	H_2 (111.3 mmol $g^{-1}\ h^{-1}$) CO (178.0 $\mu mol\ g^{-1}\ h^{-1}$) CH_4 (61.2 $\mu mol\ g^{-1}\ h^{-1}$)	[80]

Table 1. *Cont.*

Catalysts	Synthesis Method	Application	Band Gap (eV)	Rate of HER/CO$_2$RR	Ref.
CoP/rGO	Hydrothermal	CO$_2$RR	-	CO (47,330 µmol g^{-1} h^{-1})	[81]
CoP/CNT	Hydrothermal	CO$_2$RR	-	CO (39,510 µmol g^{-1} h^{-1})	[81]
FeP/CN	Thermal decomposition	CO$_2$RR	2.40	CO (5.19 µmol g^{-1} h^{-1})	[83]
NiCoP/g-C$_3$N$_4$	Thermal polymerization	HER	2.69	5162 µmol g^{-1} h^{-1}	[85]
Ni-MoP@NP$_{PF}$	Electrospinning	CO$_2$RR	1.42	CO (953.53 µmol g^{-1} h^{-1})	[86]
WP-NC/g-C$_3$N$_4$	Facile sonication	CO$_2$RR	2.8	CO (376 µmol g^{-1}h^{-1})	[93]
WP-NC/g-C$_3$N$_4$	Thermal polymerization	HER	~2.8	1217.6 µmol g^{-1} h^{-1}	[96]
Fe doped CoP	Self-assembly	CO$_2$RR	-	CO (21.0 µmol h^{-1})	[97]
NiCoP nanosheets	Wet chemical and phosphorization	HER	-	238.2 mmol g^{-1} h^{-1}	[98]
FeP/CdS	Solvothermal	HER	2.32	37.92 mmol g^{-1} h^{-1}	[99]

6. TMP Electrocatalysts for HER via Water Splitting

Over the last few years, a colossal number of attempts have been dedicated to the advancement of TMP-based electrocatalysts for propelling the applications of HER, and considerably accomplishments have been achieved by ameliorating the final results through heteroatom doping and nanostructure engineering [100–102]. Li et al. [74] synthesized Co$_2$P/Ni$_2$P nanohybrids for HER via water splitting. The as-developed nanohybrids required a very low overpotential (51 mV) to achieve 10 mA cm^{-2} alongside noteworthy operational durabilities. This catalytic performance exceeded most of the reported non-noble TMP-based electrocatalysts. The exceptional results could be attributed to the large surface area, an abundance of active sites, and robust interfacial contact between Ni$_2$P and Co$_2$P. In another reported study, Cho et al. [75] examined the HER activity of Co-, Ni-, and Mn-doped FeP nanoparticles. The electrochemical results showed that Co-FeP nanoparticles required a 126 mV overpotential to attain 10 mA cm^{-2} and exhibited higher cathodic current density than Ni- and Mn-doped FeP because of their fast charge transfer rate and high, electrochemically active surface area. In another study, Co-, Fe-, Mn-, Na-, Cr-, Li-, V-, Nb-, Ti-, Pb-, and Sn-doped Ni$_2$P electrocatalysts were investigated by Xiong et al. [76] for their HER catalytic activity. The electrochemical results demonstrated that Fe- and Co-doped Ni$_2$P exhibited superior performances similar to Pt-like activity with a very low overpotential of 31 mV at 10 mA cm^{-2}. These results are ascribed to the charge redistribution on the catalyst's surface, produced by the doping effect. Li et al. [103] fabricated MoP/MoNiP@C heterostructures to examine their electrochemical HER activity, and as a result, the as-prepared electrocatalyst showed remarkable performance, with a 134 mV overpotential and a 66 mV dec^{-1} Tafel slope. These excellent results can be ascribed to the synergistic effect between MoNiP and MoP nanoparticles that augmented the active sites of the catalyst. The LSV (linear sweep voltammetric) curves and Tafel plots of as-prepared electrocatalysts towards HER are illustrated in Figure 9a,b, whereas cyclic voltammetric (CV) curves and a double-layer capacitance plot of MoP/MoNiP@C are demonstrated in Figure 9c,d. As shown in Figure 9e, the MoP/MoNiP@C impedance is relatively smaller than other electrocatalysts, which corroborates the higher catalytic performance and outstanding conductivity of MoP/MoNiP@C. To examine the robustness of MoP/MoNiP@C for longer runs, stability cycles of the LSV curves were recorded for 2000 cycles, and minor changes in the cathodic curve were observed, as shown in Figure 9f. The onset of Figure 9f depicts the time-dependent current density curve of the optimized electrocatalyst. The fabrication flowchart of MoP/MoNiP@C is illustrated in Figure 10.
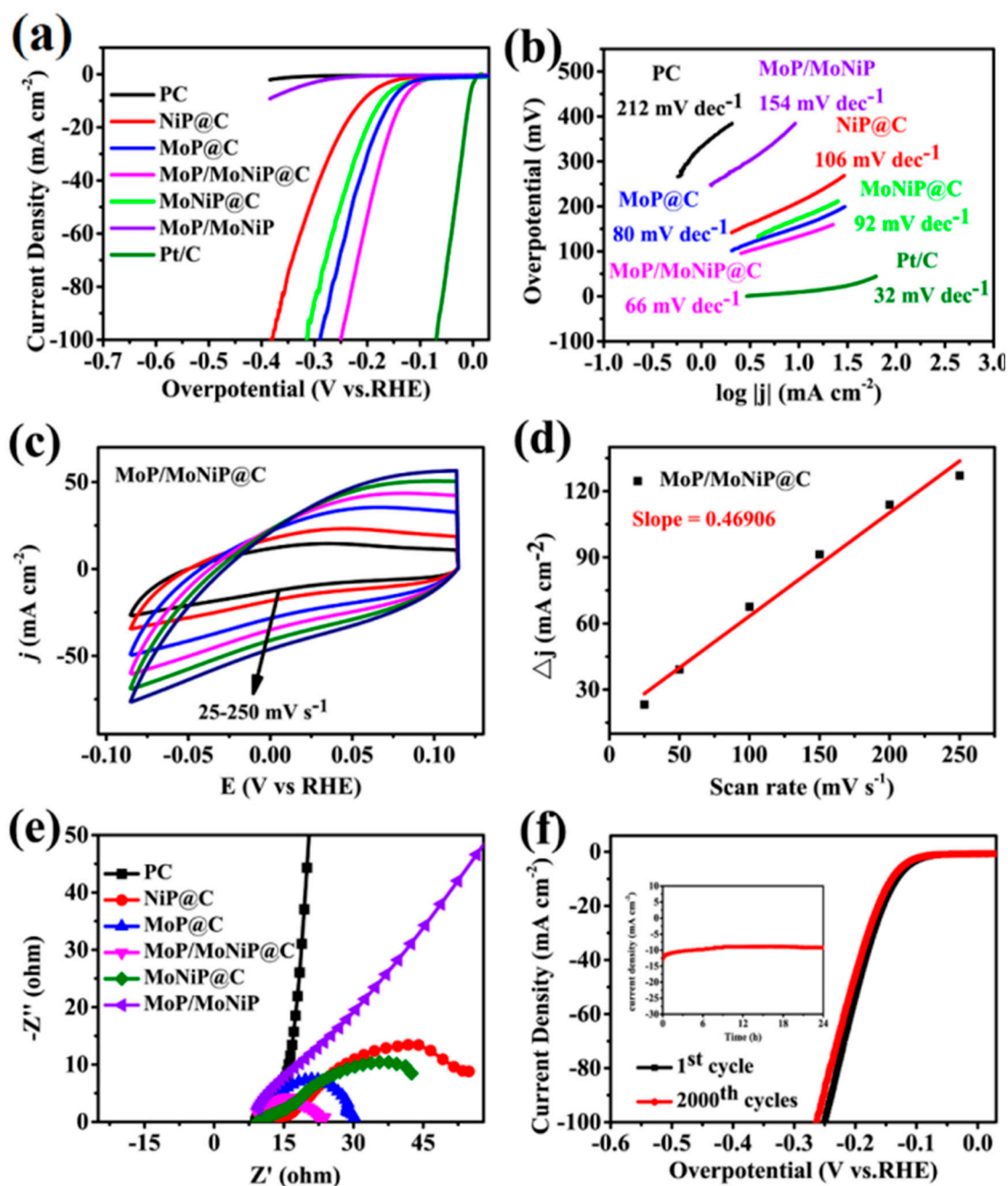
Figure 9. (**a**) LSVs of PC, NiP@C, MoP@C, MoNiP@C, MoP/MoNiP, MoP/MoNiP@C, and Pt/C in 0.5 M H_2SO_4 solution and (**b**) Tafel plots of PC, NiP@C, MoP@C, MoNiP@C, MoP/MoNiP, MoP/MoNiP@C, and Pt/C. (**c**) CV plots of MoP/MoNiP@C at a scan rates ranging from 25 to 250 mV s^{-1} and (**d**) linear fitting of Δj vs. scan rates of MoP/MoNiP@C. (**e**) EIS spectra of PC, NiP@C, MoP@CMoNiP@C, MoP/MoNiP, and MoP/MoNiP@C. (**f**) LSVs of MoP/MoNiP@C in 0.5 M H_2SO_4 before and after 1000 cycles, and the inset indicates the time-dependent current density curve at an overpotential of 140 mV for 24 h. [Reprinted with permission from Ref. [103]. Copyright 2021, American Chemical Society].
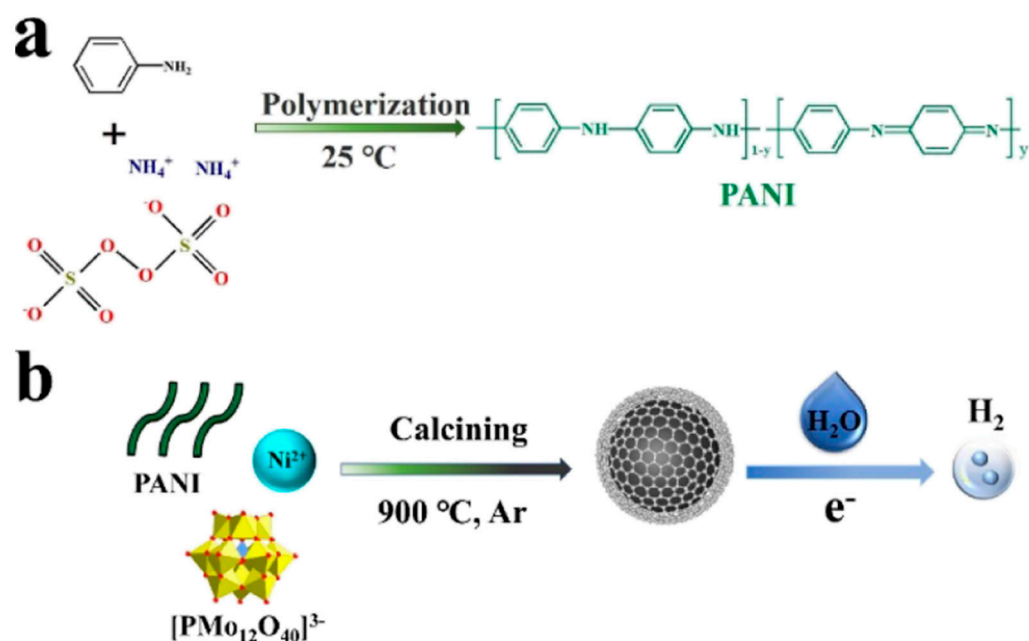
Figure 10. Synthesis Process for MoP/MoNiP@C. [Reprinted with permission from Ref. [103]. Copyright 2021, American Chemical Society].

Yang et al. [104] designed $Ni_2P/MoO_2/NF$ nanorods-type heterostructured electrocatalyst for HER water splitting. As-prepared electrocatalysts exhibited very low overpotential (34 mV), which was attributed to the combined effect between MoO_2 and Ni_2P that was enhanced due to the robust electronic coupling effect. In a reported work investigating the HER activity, Kang et al. [105] synthesized NiFeP@C electrocatalyst that showed notable results, including the low overpotential of 160 mV towards HER. The enhanced results accredited to the synergistic effect between P, Fe, Ni, and C, which accelerated the pace of charge transfer and escalated the electrocatalytic performance. Chen et al. [106] fabricated Ru-MnFeP/NF electrocatalysts to examine HER performance. The results showed a low overpotential of 35 mV alongside high stability for 50 h. Liu et al. [107] engineered Mn- and Ni-deposited FeP (Ni-Mn-FeP) electrocatalyst and investigated its HER activity. The as-prepared electrocatalyst demonstrated enhanced results with 103 mV ultralow overpotential. The combination technique of co-doped high-valence and low-valence metals motivated the advancement of high-activity and functional catalysts. In a reported study, Er-doped NiCoP/NF nanowires were fabricated by Zhang et al. [108] to assess their HER activity. The electrocatalytic efficiency of the as-prepared electrocatalyst was ascribed to its lowered overpotential value of 46 mV to reach 10 mA cm^{-2} cathodic current density. The advanced performance of Er-doped NiCoP/NF was ascribed to the amalgamation of Er to NiCoP that considerably adjusted d-band centers alongside electronic structure of Co and Ni atoms by altering to lower energies with regards to Fermi level and also enhanced the HER/OER intermediate Gibbs free energies.

7. TMP Electrocatalysts for CO$_2$RR Application

TMPs have emerged as multi-facet materials with fascinating electronic and structural features, which have led to impeccable catalytic activity for critical energy transformation such as CO_2 reduction [109,110]. There are several recent reports of electrochemical CO$_2$RR applications of TMP-based nanocatalysts. Downes et al. [111] synthesized Cu_3P nanoparticles to investigate their electrochemical CO$_2$RR performance. The results showed the formation of formate with as high as 8% Faradaic efficiency (FE). The enhanced activity and stability were accredited to using a solution-based molecular precursor method for Cu_3P fabrication that offered multi-dimensional opportunities for altering the morphology, surface chemistry, and composition to attain notable CO_2 conversion efficiency.

In another work, Ji et al. [82] incorporated FeP on a Ti mesh (FeP/TM) that functioned as an effective electrocatalyst for CO_2 reduction to transform into alcohols with 94.3% $FE_{CH3OH+C2H5OH}$ and 80.2% FE_{CH3OH}. The improved results were attributed to the combining effect between two adjacent Fe atoms, as revealed by density functional theory (DFT) calculations. Sun et al. [112] designed MoP/In-PC for electrocatalytic CO_2 reduction. The current density and FE of the as-designed electrocatalyst reached 43.8 mA cm^{-2} and 96.5%, respectively. These noteworthy results were accredited to the advantageous feature of nanosized MoP, the adsorption ability of the robust CO_2 and CO_2-intermediate, the high interfacial charge transfer, and the combining effect between In-doped carbon supports and MoP. Kim et al. [113] synthesized Ni_2P/Ho_2O_3 core–shell nanoparticles (CSNPs) to examine their scope in electrochemical CO_2RR applications. As-synthesized electrocatalysts generated acetone with 25.4% FE that was attributed to the synergistic effect between Ni_2P and Ho_2O_3. Figure 11 depicts the synthesis steps for designing Ni_2P/Ho_2O_3 catalytic systems. The four main value-added products in the form of H_2, HCOOH, CH_3OH, and $(CH_3)_2CO$ resulted from the reduction of CO_2, as revealed in the Figure 12a, Ni_2P/Ho_2O_3 core–shell nanoparticles (CSNPs) have been found to be very beneficial for the electrocatalytic behavior towards $(CH_3)_2CO$. While Ho_2O_3 nanodisks (NDs) produced H_2, HCOOH, and CH_3OH, only H_2 was generated by Ni_2P in electrocatalytic CO_2 reduction towards C_2 or C_3 pathways, as shown in Figure 12b–d.
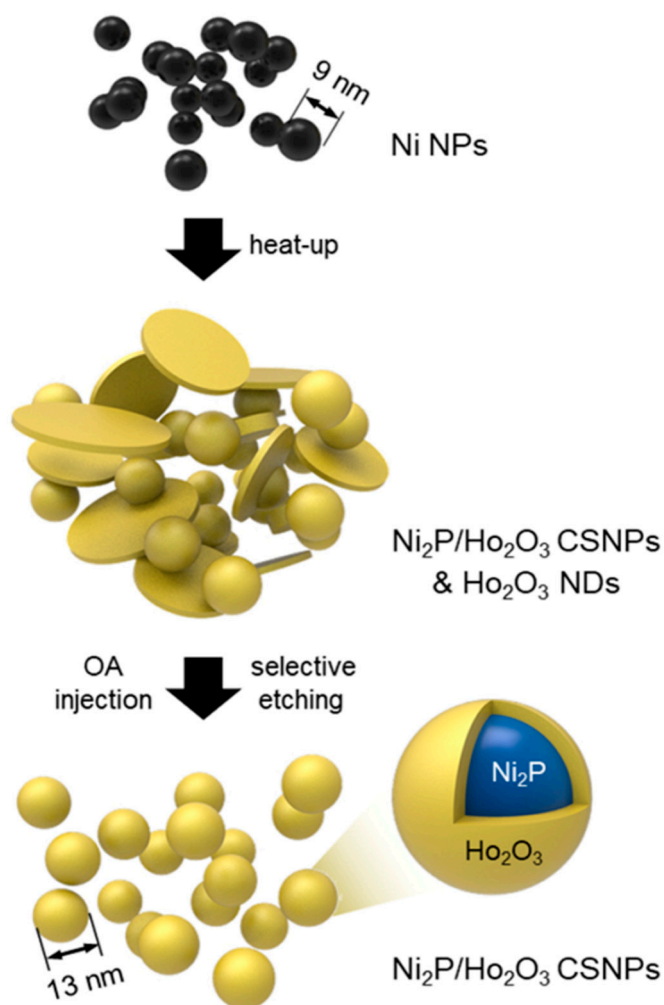

Figure 11. Schematic illustration of the experimental procedure for synthesis of C/A Ni_2P/Ho_2O_3 CSNPs (NPs, NDs, and CSNPs stand for nanoparticles, nanodisks, and core–shell nanoparticles, respectively). [Reprinted with permission from Ref. [113]. Copyright 2020, American Chemical Society].
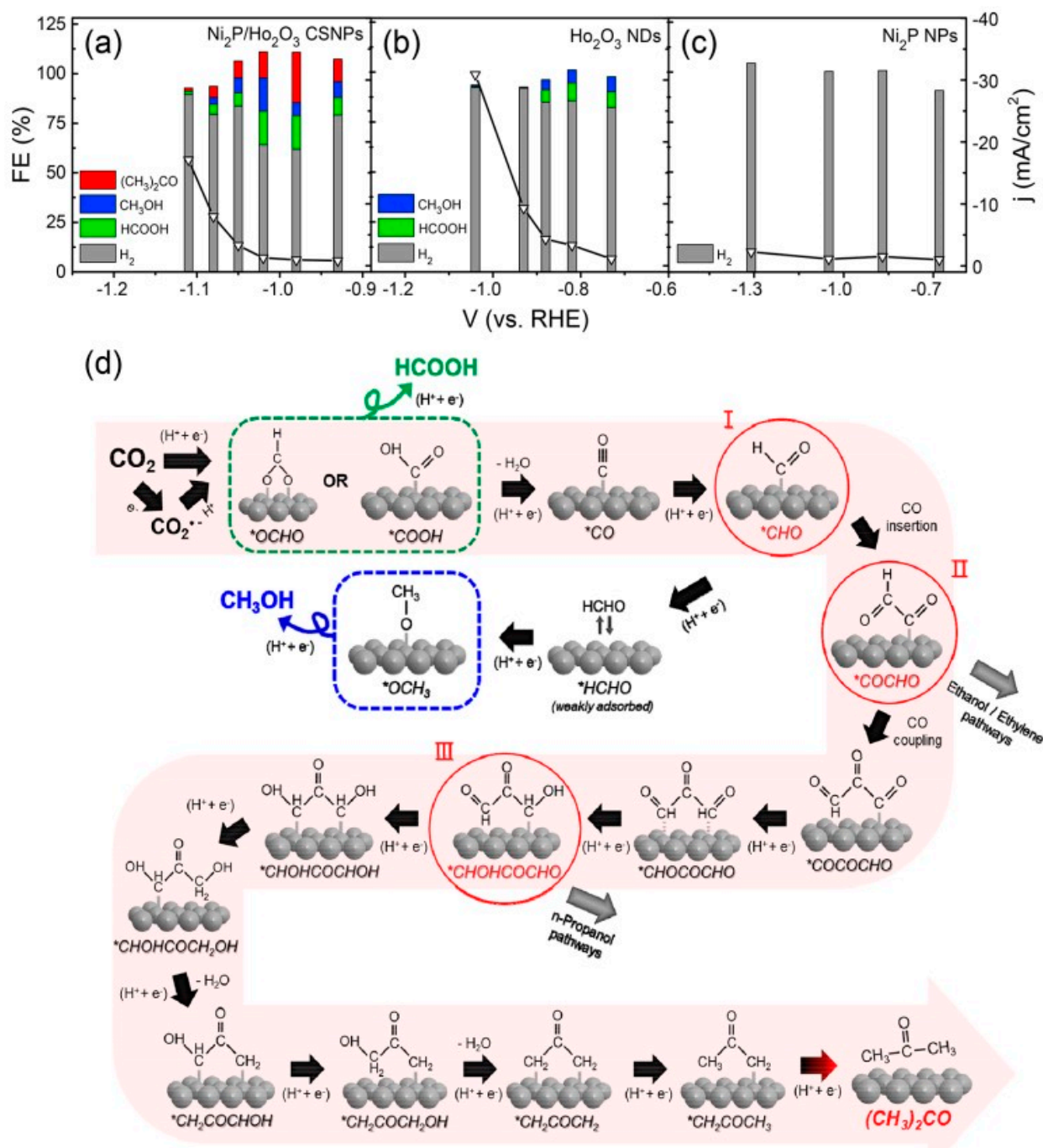
Figure 12. Potential-dependent FEs of CO_2RR products and total current densities obtained using (**a**) Ni_2P/Ho_2O_3 CSNPs, (**b**) Ho_2O_3 NDs, and (**c**) Ni_2P NPs as electrocatalysts. (**d**) Suggested CO_2RR pathways toward $(CH_3)_2CO$. [Reprinted with permission from Ref. [113]. Copyright 2020, American Chemical Society].

Laursen et al. [114] fabricated Cu_3P NS/Cu for electrocatalytic CO_2RR. The results showed the formation of formate with a 65 mV lower overpotential value and 0.9% FE. A Fe_2P electrocatalyst was synthesized by Calvinho et al. [115] to examine the CO_2 conversion efficiency. The outcomes showed a 53% FE with ethylene glycol (C_2) product formation after CO_2 reduction, which inferred successful C-C coupling during the surface adsorption reaction mechanism. Banerjee et al. [116] fabricated Ni_2P electrocatalyst for the reduction of CO_2, and the result demonstrated the formation of formaldehyde along with the surface hydrogen affinity and dynamic reconstruction of the surface through adsorption of H

that promoted the C–C coupling and selective reduction of CO_2 on Ni_2P. The catalytic proficiency of TMPs towards electrochemical HER and CO_2RR applications are tabulated in Tables 2 and 3, respectively.

Table 2. Transition-metal-phosphide-based electrocatalysts for HER application.

Electrocatalyst	Synthesis Method	Application	Overpotential (mV)	Tafel Slope (mV dec^{-1})	Ref.
Co_2P/Ni_2P	Thermal phosphorization	HER	51	-	[74]
Co-FeP	Phosphorization	HER	126	63.6	[75]
Co-Ni$_2$P	Synthetic method	HER	31	47	[76]
MoP/MoNiP@C	Calcination and phosphorization	HER	134	66	[103]
Ni$_2$P/MoO$_2$/NF	Phosphorization	HER	34	45.8	[104]
NiFeP@C	Calcination	HER	160	75.8	[105]
Ru-MnFeP/NF	Phosphorization	HER	35	69	[106]
Ni-Mn-FeP	Phosphorization	HER	103	-	[107]
Er-NiCoP/NF	Phosphorization	HER	46	-	[108]

Table 3. Transition-metal-phosphide-based electrocatalysts for CO_2RR application.

Electrocatalysts	Synthesis Method	Power Density/ Current Density	Faradaic Efficiency	Ref.
Cu$_3$P/C	Hydrothermal	2.6 mW cm^{-2}	47% (CO)	[28]
AgP$_2$	Self-assembly	−8.7 mA cm^{-2}	82.0% (CO)	[63]
FeP/TM	Hydrothermal	-	94.3% (CH$_3$OH + C$_2$H$_5$OH)	[82]
Cu$_3$P	Thermal decomposition	-	8% (Formate)	[111]
MoP@In-PC	Solid state	43.8 mA cm^{-2}	96.5% (HCOOH)	[112]
Ni$_2$P/Ho$_2$O$_3$	Phosphorization	0.95 mA cm^{-2}	25.4% (Acetone)	[113]
Cu$_3$P NS/Cu	Self-assembly	-	1.1% ± 0.6% (Formic acid)	[114]
TiO$_2$/MnP	Annealing	-	67% ± 5% (CO) 12.4% ± 1.4% (H$_2$)	[117]

The aforementioned path-breaking reports are proof for the ongoing research on TMPs as cocatalyst or electrocatalyst in HER via water splitting and CO_2RR applications. However, there are still many mysteries unsolved regarding the synthesis of TMPs that comprise tail gas post-treatment and unstable reactants, which create obstacles for the bright future of TMPs as electrocatalysts. Therefore, coping with these bottlenecks of TMP nanostructures can simplify their success in energy-driven catalytic applications at scalable points.

8. Future Perspectives

The outlook of nanocatalysis-assisted HER and CO_2RR is propitious thanks to wide array of physicochemical modulations that can be carried out in different nanomaterials. Alleviating the cost of green HER and CO_2RR applications is fundamental for applying these sustainable pathways to a scalable utility in day-to-day life. Therefore, designing cheap catalytic systems as an economical substitute for noble metal catalysts is the need

of the hour in order to cope up with the latter's whopping costs, which currently hinders the widespread exploitation of green HER and CO_2RR applications [117–120]. In the last few years, researchers have realized the potential of TMPs as tremendously efficient catalytic systems able to address the energy related applications at scalable points [121–124]. Extensive energy-focused research operations have been performed by employing TMP nanostructured catalytic systems [125]. TMPs are emerging advanced functional materials that have recently exhibited great potential in catalyzing HER and CO_2RR to generate value-added chemicals and fuels [126–128]. On account of their versatile physicochemical properties, TMPs are beneficial in a broad range of applications, varying from catalysis to energy storage devices. TMPs come forth as remarkable catalytic systems which offer a high range of performances and great robustness. Their inexpensiveness and recent ground-breaking advances promise to fill the void between research and commercial applicability.

Experimental and computational investigations of TMP nanostructures highlight their marvelous catalytic efficiency, stability, and selectivity towards HER and CO_2RR applications [129]. However, the extent of their catalysis hinges upon exposed active sites, which govern the surface adsorption reactions. Therefore, it is fundamentally important to enhance the interaction between TMPs' surface sites and the reactant molecules to escalate the turnover frequency of generating H_2 and another chemical feedstock [130]. One major bottleneck of TMP-assisted nanocatalysis is the scarcity of reports which systematically explore and elucidate the reaction mechanism behind their inherent catalytic proficiency at an atomic scale. To examine the in-situ behavior of TMPs, sophisticated characterization techniques such as X-ray absorption and operando and in situ Raman spectroscopies can be upgraded in accordance with the reaction conditions for probing the intermediate steps involved during HER and CO_2RR applications. In addition, theoretical models should be developed to determine the thermodynamic landscape and kinetics of surface reactions on the active TMPs centers.

9. Conclusions

Herein, we have discussed the exigency of renewable energy-driven H_2 production and CO_2 sequestration in order to meet the current energy demand through clean energy resources. TMP nanocatalysts have been reviewed as heterogeneous catalytic systems for HER and CO_2RR applications. The structural advantages of TMPs have been discussed precisely, as structural engineering is one of the most sought-after pathways for enhancing their activity and stability. To understand the structural significance of TMPs, the role of P and M/P ratio was reviewed. We have summarized the most utilized synthetic methodologies for designing TMP nanostructures. Photocatalytic HER and CO_2RR applications were surveyed collectively under the enlightenment of recent achievements of TMPs. Bimetallic NiCoP exhibits an enormous rate of H_2 production (238.2 mmol g^{-1} h^{-1}), and heterostructured CoP/rGO was found to have a higher rate of reducing CO_2 to CO (47.33 mmol g^{-1} h^{-1}). Correspondingly, recent advances in electrocatalytic HER and CO_2RR applications were also reviewed, which corroborate the diverse applicability of TMP nanocatalysts in energy-driven applications. Pristine Ni_2P has emerged as a resourceful electrocatalyst for HER. Nevertheless, there are only a handful reports for electrocatalytic CO_2 reduction, which is at the cutting edge of technology and needs to be developed further in future environmental aspirations. For CO_2RR applications, TMPs can be exploited in either gas-phase or liquid-phase reactions, which facilitate the conversion of CO_2 into chemical feedstocks such as C_1 and C_2 products and other higher hydrocarbons. The P content and physicochemical properties of TMPs play major roles in regulating their catalytic responses. Therefore, optimizing reaction conditions and synthetic routes is instrumental in developing these emerging functional materials for energy-related applications. TMPs can be a game-changer in the field of nanocatalysis thanks to their Earth-abundance and cost-effectiveness.

References

1. Ali, S.A.; Sadiq, I.; Ahmad, T. Oxide based Heterostructured Photocatalysts for CO_2 Reduction and Hydrogen Generation. *ChemistrySelect* **2023**, *8*, 202203176. [CrossRef]
2. Moutinho, V.; Madaleno, M.; Inglesi-Lotz, R.; Dogan, E. Factors affecting CO_2 emissions in top countries on renewable energies: A LMDI decomposition application. *Renew. Sustain. Energy Rev.* **2018**, *90*, 605–622. [CrossRef]
3. Waheed, R.; Chang, D.; Sarwar, S.; Chen, W. Forest, agriculture, renewable energy, and CO_2 emission. *J. Clean. Prod.* **2018**, *172*, 4231–4238. [CrossRef]
4. Leggett, J.A. *The United Nations Framework Convention on Climate Change, the Kyoto Protocol, and the Paris Agreement: A Summary*; UNFCC: New York, NY, USA, 2020; p. 2.
5. Chiodi, A.M.; Harrison, D.E. Comment on Qian et al. La Niña and El Niño composites of atmospheric CO_2 change. *Tellus B Chem. Phys. Meteorol.* **2014**, *66*, 20428. [CrossRef]
6. Ali, S.A.; Ahmad, T. Treasure trove for efficient hydrogen evolution through water splitting using diverse perovskite photocatalysts. *Mater. Today Chem.* **2023**, *29*, 101387. [CrossRef]
7. Shaheen, S.; Sadiq, I.; Ali, S.A.; Ahmad, T. Bismuth-Based Multi-Component Heterostructured Nanocatalysts for Hydrogen Generation. *Catalysts* **2023**, *13*, 295. [CrossRef]
8. Abdalla, A.M.; Hossain, S.; Nisfindy, O.B.; Azad, A.T.; Dawood, M.; Azad, A.K. Hydrogen production, storage, transportation and key challenges with applications: A review. *Energy Convers. Manag.* **2018**, *165*, 602–627. [CrossRef]
9. Naaz, F.; Alshehri, S.M.; Mao, Y.; Ahmad, T. Unraveling the chemoselective catalytic, photocatalytic and electrocatalytic applications of copper supported WO_3 nanosheets. *Catal. Commun.* **2023**, *178*, 106678. [CrossRef]
10. Sadiq, I.; Ali, S.A.; Ahmad, T. Graphene-Based Derivatives Heterostructured Catalytic Systems for Sustainable Hydrogen Energy via Overall Water Splitting. *Catalysts* **2023**, *13*, 109. [CrossRef]
11. Singla, S.; Sharma, S.; Basu, S.; Shetti, N.P.; Aminabhavi, T.M. Photocatalytic water splitting hydrogen production via environmental benign carbon-based nanomaterials. *Int. J. Hydrogen Energy* **2021**, *46*, 33696–33717. [CrossRef]
12. Ramadoss, M.; Chen, Y.; Chen, X.; Su, Z.; Karpuraranjith, M.; Yang, D.; Pandit, M.A.; Muralidharan, K. Iron-modulated three-dimensional CoNiP vertical nanoarrays: An exploratory binder-free bifunctional electrocatalyst for efficient overall water splitting. *J. Phys. Chem. C* **2021**, *125*, 20972–20979. [CrossRef]
13. Shi, Y.; Zhang, B. Recent advances in transition metal phosphide nanomaterials: Synthesis and applications in hydrogen evolution reaction. *Chem. Soc. Rev.* **2016**, *45*, 1529–1541. [CrossRef] [PubMed]
14. Dong, Y.; Kong, L.; Jiang, P.; Wang, G.; Zhao, N.; Zhang, H.; Tang, B. A general strategy to fabricate Ni_xP as highly efficient cocatalyst via photoreduction deposition for hydrogen evolution. *ACS Sustain. Chem. Eng.* **2017**, *5*, 6845–6853. [CrossRef]
15. Landers, A.T.; Fields, M.; Torelli, D.A.; Xiao, J.; Hellstern, T.R.; Francis, S.A.; Tsai, C.; Kibsgaard, J.; Lewis, N.S.; Chan, K.; et al. The predominance of hydrogen evolution on transition metal sulfides and phosphides under CO_2 reduction conditions: An experimental and theoretical study. *ACS Energy Lett.* **2018**, *3*, 1450–1457. [CrossRef]
16. Li, Y.; Sun, Y.; Qin, Y.; Zhang, W.; Wang, L.; Luo, M.; Yang, H.; Guo, S. Recent advances on water-splitting electrocatalysis mediated by noble-metal-based nanostructured materials. *Adv. Energy Mater.* **2020**, *10*, 1903120. [CrossRef]
17. Stolarczyk, J.K.; Bhattacharyya, S.; Polavarapu, L.; Feldmann, J. Challenges and prospects in solar water splitting and CO_2 reduction with inorganic and hybrid nanostructures. *ACS Catal.* **2018**, *8*, 3602–3635. [CrossRef]
18. Pandit, N.A.; Ahmad, T. Tin Oxide Based Hybrid Nanostructures for Efficient Gas Sensing. *Molecules* **2022**, *27*, 7038. [CrossRef]
19. Vaidya, S.; Ahmad, T.; Agarwal, S.; Ganguli, A.K. Nanocrystalline oxalate/carbonate precursors of Ce and Zr and their decompositions to CeO_2 and ZrO_2 nanoparticles. *J. Am. Ceram. Soc.* **2007**, *90*, 863–869. [CrossRef]
20. Ahmad, T.; Ganguli, A.K. Structural and dielectric characterization of nanocrystalline (Ba, Pb) ZrO_3 developed by reverse micellar synthesis. *J. Am. Ceram. Soc.* **2006**, *89*, 3140–3146. [CrossRef]

21. Ahmad, T.; Shahazad, M.; Ubaidullah, M.; Ahmed, J.; Khan, A.; El-Toni, A.M. Structural characterization and dielectric properties of ceria–titania nanocomposites in low ceria region. *Mater. Res. Express* **2017**, *4*, 125016. [CrossRef]

22. Ganguli, A.K.; Vaidya, S.; Ahmad, T. Synthesis of nanocrystalline materials through reverse micelles: A versatile methodology for synthesis of complex metal oxides. *Bull. Mater. Sci.* **2008**, *31*, 415–419. [CrossRef]

23. Ahmad, T.; Lone, I.H.; Ubaidullah, M. Structural characterization and multiferroic properties of hexagonal nano-sized YMnO$_3$ developed by a low temperature precursor route. *RSC Adv.* **2015**, *5*, 58065–58071. [CrossRef]

24. Fazil, M.; Ahmad, T. Pristine TiO$_2$ and Sr-Doped TiO$_2$ Nanostructures for Enhanced Photocatalytic and Electrocatalytic Water Splitting Applications. *Catalysts* **2023**, *13*, 93. [CrossRef]

25. Zhang, M.; Xu, Y.; Williams, B.L.; Xiao, M.; Wang, S.; Han, D.; Sun, L.; Meng, Y. Catalytic materials for direct synthesis of dimethyl carbonate (DMC) from CO$_2$. *J. Clean. Prod.* **2021**, *279*, 123344. [CrossRef]

26. Chauhan, D.K.; Sharma, N.; Kailasam, K. A critical review on emerging photocatalysts for syngas generation via CO$_2$ reduction under aqueous medium: A sustainable paradigm. *Adv. Mater.* **2022**, *3*, 5274–5298. [CrossRef]

27. Zaza, L.; Rossi, K.; Buonsanti, R. Well-defined copper-based nanocatalysts for selective electrochemical reduction of CO$_2$ to C2 products. *ACS Energy Lett.* **2022**, *7*, 1284–1291. [CrossRef]

28. Kim, D.; Kley, C.S.; Li, Y.; Yang, P. Copper nanoparticle ensembles for selective electroreduction of CO$_2$ to C2–C3 products. *Proc. Natl. Acad. Sci. USA* **2017**, *114*, 10560–10565. [CrossRef]

29. Tu, W.; Zhou, Y.; Zou, Z. Photocatalytic conversion of CO$_2$ into renewable hydrocarbon fuels: State-of-the-art accomplishment, challenges, and prospects. *Adv. Mater.* **2014**, *26*, 4607–4626. [CrossRef]

30. Khan, H.; Lone, I.H.; Lofland, S.E.; Ramanujachary, K.V.; Ahmad, T. Exploiting multiferroicity of TbFeO$_3$ nanoparticles for hydrogen generation through photo/electro/photoelectro-catalytic water splitting. *Int. J. Hydrogen Energy* **2023**, *48*, 5493–5505. [CrossRef]

31. Liu, L.; Corma, A. Structural transformations of solid electrocatalysts and photocatalysts. *Nat. Rev. Chem.* **2021**, *5*, 256–276. [CrossRef]

32. Fazil, M.; Alshehri, S.M.; Mao, Y.; Ahmad, T. Hydrothermally Derived Mg-Doped TiO$_2$ Nanostructures for Enhanced H$_2$ Evolution Using Photo-and Electro-Catalytic Water Splitting. *Catalysts* **2023**, *13*, 893. [CrossRef]

33. Moon, S.Y.; Gwag, E.H.; Park, J.Y. Hydrogen Generation on Metal/Mesoporous Oxides: The Effects of Hierarchical Structure, Doping, and Co-catalysts. *Energy Technol.* **2018**, *6*, 459–469. [CrossRef]

34. Mamiyev, Z.; Balayeva, N.O. Metal Sulfide Photocatalysts for Hydrogen Generation: A Review of Recent Advances. *Catalysts* **2022**, *12*, 1316. [CrossRef]

35. Zhang, H.; Li, J.; Tan, Q.; Lu, L.; Wang, Z.; Wu, G. Metal–organic frameworks and their derived materials as electrocatalysts and photocatalysts for CO$_2$ reduction: Progress, challenges, and perspectives. *Chem. Eur. J.* **2018**, *24*, 18137–18157. [CrossRef]

36. Ali, S.A.; Ahmad, T. Chemical strategies in molybdenum-based chalcogenides nanostructures for photocatalysis. *Int. J. Hydrogen Energy* **2022**, *47*, 29255–29283. [CrossRef]

37. Kuang, P.; Sayed, M.; Fan, J.; Cheng, B.; Yu, J. 3D graphene-based H$_2$-production photocatalyst and electrocatalyst. *Adv. Energy Mater.* **2020**, *10*, 1903802. [CrossRef]

38. Mehtab, A.; Alshehri, S.M.; Ahmad, T. Photocatalytic and photoelectrocatalytic water splitting by porous g-C$_3$N$_4$ nanosheets for hydrogen generation. *ACS Appl. Nano Mater.* **2022**, *5*, 12656–12665. [CrossRef]

39. Hameed, R.A. Nanostructured Phosphides as Electrocatalysts for Green Energy Generation. In *Noble Metal-Free Electrocatalysts: New Trends in Electrocatalysts for Energy Applications*; American Chemical Society: Washington, DC, USA, 2022; pp. 191–235.

40. Meng, S.; An, P.; Chen, L.; Sun, S.; Xie, Z.; Chen, M.; Jiang, D. Integrating Ru-modulated CoP nanosheets binary co-catalyst with 2D g-C$_3$N$_4$ nanosheets for enhanced photocatalytic hydrogen evolution activity. *J. Colloid Interface Sci.* **2021**, *585*, 108–117. [CrossRef] [PubMed]

41. Cao, S.; Wang, C.J.; Fu, W.F.; Chen, Y. Metal phosphides as co-catalysts for photocatalytic and photoelectrocatalytic water splitting. *ChemSusChem* **2017**, *10*, 4306–4323. [CrossRef]

42. Theerthagiri, J.; Murthy, A.P.; Lee, S.J.; Karuppasamy, K.; Arumugam, S.R.; Yu, Y.; Hanafiah, M.M.; Kim, H.S.; Mittal, V.; Choi, M.Y. Recent progress on synthetic strategies and applications of transition metal phosphides in energy storage and conversion. *Ceram. Int.* **2021**, *47*, 4404–4425. [CrossRef]

43. Fang, Y.; Flake, J.C. Electrochemical reduction of CO$_2$ at functionalized Au electrodes. *J. Am. Chem. Soc.* **2017**, *139*, 3399–3405. [CrossRef]

44. Antil, B.; Kumar, L.; Das, M.R.; Deka, S. Incorporating NiCoP Cocatalyst into Hollow Rings of ZnCo-Metal–Organic Frameworks to Deliver Pt Cocatalyst like Visible Light Driven Hydrogen Evolution Activity. *ACS Appl. Energy Mater.* **2022**, *5*, 11113–11121. [CrossRef]

45. Koshy, D.M.; Akhade, S.A.; Shugar, A.; Abiose, K.; Shi, J.; Liang, S.; Oakdale, J.S.; Weitzner, S.E.; Varley, J.B.; Duoss, E.B.; et al. Chemical modifications of Ag catalyst surfaces with imidazolium ionomers modulate H$_2$ evolution rates during electrochemical CO$_2$ reduction. *J. Am. Chem. Soc.* **2021**, *143*, 14712–14725. [CrossRef]

46. Liu, Y.; Li, X.; He, H.; Yang, S.; Jia, G.; Liu, S. CoP imbedded g-C$_3$N$_4$ heterojunctions for highly efficient photo, electro and photoelectrochemical water splitting. *J. Colloid Interface Sci.* **2021**, *599*, 23–33. [CrossRef] [PubMed]

47.　Guo, F.; Huang, X.; Chen, Z.; Sun, H.; Chen, L. Prominent co-catalytic effect of CoP nanoparticles anchored on high-crystalline g-C_3N_4 nanosheets for enhanced visible-light photocatalytic degradation of tetracycline in wastewater. *J. Chem. Eng.* **2020**, *395*, 125118. [CrossRef]

48.　Sun, Z.; Zhu, M.; Fujitsuka, M.; Wang, A.; Shi, C.; Majima, T. Phase Effect of Ni_xP_y Hybridized with g-C_3N_4 for Photocatalytic Hydrogen Generation. *ACS Appl. Mater. Interfaces* **2017**, *9*, 30583–30590. [CrossRef] [PubMed]

49.　Sun, Y.; Wang, S.; Jiao, D.; Li, F.; Qiu, S.; Wang, Z.; Cai, Q.; Zhao, J.; Sun, C. Two-dimensional Pt_2P_3 monolayer: A promising bifunctional electrocatalyst with different active sites for hydrogen evolution and CO_2 reduction. *Chin. Chem. Lett.* **2022**, *33*, 3987–3992. [CrossRef]

50.　Sun, M.; Liu, H.; Qu, J.; Li, J. Earth-rich transition metal phosphide for energy conversion and storage. *Adv. Energy Mater.* **2016**, *6*, 1600087. [CrossRef]

51.　Zhao, H.; Yuan, Z.Y. Insights into transition metal phosphate materials for efficient electrocatalysis. *ChemCatChem* **2020**, *12*, 3797–3810. [CrossRef]

52.　Jiao, Y.Q.; Yan, H.J.; Tian, C.G.; Fu, H.G. Structure Engineering and Electronic Modulation of Transition Metal Interstitial Compounds for Electrocatalytic Water Splitting. *Acc. Chem. Res.* **2022**, *4*, 42–56. [CrossRef]

53.　Huang, C.J.; Xu, H.M.; Shuai, T.Y.; Zhan, Q.N.; Zhang, Z.J.; Li, G.R. A review of modulation strategies for improving catalytic performance of transition metal phosphides for oxygen evolution reaction. *Appl. Catal. B* **2022**, *325*, 122313. [CrossRef]

54.　He, R.; Huang, X.; Feng, L. Recent progress in transition-metal sulfide catalyst regulation for improved oxygen evolution reaction. *Energy Fuels* **2022**, *36*, 6675–6694. [CrossRef]

55.　Oyama, S.T.; Gott, T.; Zhao, H.; Lee, Y.K. Transition metal phosphide hydro processing catalysts: A review. *J. Catal. Today* **2009**, *143*, 94–107. [CrossRef]

56.　Gong, N.; Deng, C.; Wu, L.; Wan, B.; Wang, Z.; Li, Z.; Gou, H.; Gao, F. Structural diversity and electronic properties of 3d transition metal tetraphosphides, TMP_4 (TM= V, Cr, Mn, and Fe). *Inorg. Chem.* **2018**, *57*, 9385–9392. [CrossRef] [PubMed]

57.　Lakshmy, S.; Santhosh, S.; Kalarikkal, N.; Rout, C.S.; Chakraborthy, B. A review of electrochemical glucose sensing based on transition metal phosphides. *J. Appl. Phys.* **2023**, *133*, 070702. [CrossRef]

58.　Kuo, D.Y.; Nishiwaki, E.; Rivera-Maldonado, R.A.; Cossairt, B.M. The Role of Hydrogen Adsorption Site Diversity in Catalysis on Transition-Metal Phosphide Surfaces. *ACS Catal.* **2022**, *13*, 287–295. [CrossRef]

59.　Shi, Y.; Li, M.; Yu, Y.; Zhang, B. Recent advances in nanostructured transition metal phosphides: Synthesis and energy-related applications. *Energy Environ. Sci.* **2020**, *13*, 4564–4582. [CrossRef]

60.　Weng, B.; Wei, W.; Wu, H.; Alenizi, A.M.; Zheng, G. Bifunctional CoP and CoN porous nanocatalysts derived from ZIF-67 in situ grown on nanowire photoelectrodes for efficient photoelectrochemical water splitting and CO_2 reduction. *J. Mater. Chem. A* **2016**, *4*, 15353–15360. [CrossRef]

61.　Lin, L.; Piao, S.; Choi, Y.; Lyu, L.; Hong, H.; Kim, D.; Lee, J.; Zhang, W.; Piao, Y. Nanostructured transition metal nitrides as emerging electrocatalysts for water electrolysis: Status and challenges. *EnergyChem* **2022**, *4*, 100072. [CrossRef]

62.　Zhong, Y.; Yin, L.; He, P.; Liu, W.; Wu, Z.; Wang, H. Surface chemistry in cobalt phosphide-stabilized lithium–sulfur batteries. *J. Am. Chem. Soc.* **2018**, *140*, 1455–1459. [CrossRef]

63.　Li, H.; Wen, P.; Itanze, D.S.; Hood, Z.D.; Ma, X.; Kim, M.; Adhikari, S.; Lu, C.; Dun, C.; Chi, M.; et al. Colloidal silver diphosphide (AgP_2) nanocrystals as low overpotential catalysts for CO_2 reduction to tunable syngas. *Nat. Commun.* **2019**, *10*, 5724. [CrossRef]

64.　Hu, E.; Feng, Y.; Nai, J.; Zhao, D.; Hu, Y.; Lou, X.W.D. Construction of hierarchical Ni–Co–P hollow nanobricks with oriented nanosheets for efficient overall water splitting. *Energy Environ. Sci* **2018**, *11*, 872–880. [CrossRef]

65.　Shi, Y.; Zhang, B. Engineering transition metal phosphide nanomaterials as highly active electrocatalysts for water splitting. *J. Chem. Soc. Dalton Trans.* **2017**, *46*, 16770–16773. [CrossRef] [PubMed]

66.　Xu, J.; Xiong, D.; Amorim, I.; Liu, L. Template-free synthesis of hollow iron phosphide–phosphate composite nanotubes for use as active and stable oxygen evolution electrocatalysts. *ACS Appl. Nano Mater.* **2018**, *1*, 617–624. [CrossRef]

67.　Yang, Y.; Luo, M.; Xing, Y.; Wang, S.; Zhang, W.; Lv, F.; Li, Y.; Zhang, Y.; Wang, W.; Guo, S. A Universal Strategy for Intimately Coupled Carbon Nanosheets/MoM Nanocrystals (M= P, S, C, and O) Hierarchical Hollow Nanospheres for Hydrogen Evolution Catalysis and Sodium-Ion Storage. *J. Adv. Mater.* **2018**, *30*, 1706085.

68.　Wu, T.; Pi, M.; Wang, X.; Guo, W.; Zhang, D.; Chen, S. Hierarchical cobalt poly-phosphide hollow spheres as highly active and stable electrocatalysts for hydrogen evolution over a wide pH range. *Appl. Surf. Sci.* **2018**, *427*, 800–806. [CrossRef]

69.　Yang, S.; Chen, G.; Ricciardulli, A.G.; Zhang, P.; Zhang, Z.; Shi, H.; Ma, J.; Zhang, J.; Blom, P.W.; Feng, X. Topochemical Synthesis of Two-Dimensional Transition-Metal Phosphides Using Phosphorene Templates. *Angew. Chem. Int. Edi.* **2020**, *59*, 465–470. [CrossRef]

70.　Zong, Q.; Liu, C.; Yang, H.; Zhang, Q.; Cao, G. Tailoring nanostructured transition metal phosphides for high-performance hybrid supercapacitors. *Nano Today* **2021**, *38*, 101201. [CrossRef]

71.　Su, J.; Zhou, J.; Wang, L.; Liu, C.; Chen, Y. Synthesis and application of transition metal phosphides as electrocatalyst for water splitting. *Sci. Bull.* **2017**, *62*, 633–644. [CrossRef]

72.　Li, Q.; Feng, W.; Liu, Y.; Chen, D.; Wu, Z.; Wang, H. Synergistic effect of spatially isolated Ni_2P and NiO redox cocatalysts on g-C_3N_4 for sustainably boosted CO_2 photocatalytic reduction. *J. Mater. Chem. A* **2022**, *10*, 15752–15765. [CrossRef]

73. Liu, Z.; Yang, S.; Sun, B.; Chang, X.; Zheng, J.; Li, X. A peapod-like CoP@ C nanostructure from phosphorization in a low-temperature molten salt for high-performance lithium-ion batteries. *Angew. Chem. Int. Ed. Engl.* **2018**, *57*, 10187–10191. [CrossRef] [PubMed]

74. Li, D.Y.; Liao, L.L.; Zhou, H.Q.; Zhao, Y.; Cai, F.M.; Zeng, J.S.; Liu, F.; Wu, H.; Tang, D.S.; Yu, F. Highly active non-noble electrocatalyst from Co_2P/Ni_2P nanohybrids for pH-universal hydrogen evolution reaction. *Mater. Today Phys.* **2021**, *16*, 100314. [CrossRef]

75. Cho, G.; Park, Y.; Kang, H.; Hong, Y.K.; Lee, T.; Ha, D.H. Transition metal-doped FeP nanoparticles for hydrogen evolution reaction catalysis. *Appl. Surf. Sci.* **2020**, *510*, 145427. [CrossRef]

76. Xiong, L.; Wang, B.; Cai, H.; Hao, H.; Li, J.; Yang, T.; Yang, S. Understanding the doping effect on hydrogen evolution activity of transition-metal phosphides: Modeled with Ni_2P. *Appl. Catal. B* **2021**, *295*, 120283. [CrossRef]

77. Ye, C.; Wang, M.Q.; Chen, G.; Deng, Y.H.; Li, L.J.; Luo, H.Q.; Li, N.B. One-step CVD synthesis of carbon framework wrapped Co_2P as a flexible electrocatalyst for efficient hydrogen evolution. *J. Mater. Chem. A* **2017**, *5*, 7791–7795. [CrossRef]

78. Li, X.L.; Wang, X.J.; Zhu, J.Y.; Li, Y.P.; Zhao, J.; Li, F.T. Fabrication of two-dimensional $Ni_2P/ZnIn_2S_4$ heterostructures for enhanced photocatalytic hydrogen evolution. *J. Chem. Eng.* **2018**, *353*, 15–24. [CrossRef]

79. Sun, W.; Fu, Z.; Shi, H.; Jin, C.; Liu, E.; Zhang, X.; Fan, J. Cu_3P and Ni_2P co-modified $g-C_3N_4$ nanosheet with excellent photocatalytic H_2 evolution activities. *J. Chem. Technol. Biotechnol.* **2020**, *95*, 3117–3125. [CrossRef]

80. Su, L.; Chen, M.; Zhang, H.; Tu, W. Construction of porous Ni_2P cocatalyst and its promotion effect on photocatalytic H2 production reaction and CO_2 reduction. *Int. J. Hydrogen Energy* **2023**, *48*, 15105–15116. [CrossRef]

81. Fu, Z.C.; Xu, R.C.; Moore, J.T.; Liang, F.; Nie, X.C.; Mi, C.; Mo, J.; Xu, Y.; Xu, Q.Q.; Yang, Z.; et al. Highly Efficient Photocatalytic System Constructed from CoP/Carbon Nanotubes or Graphene for Visible-Light-Driven CO_2 Reduction. *Chem. Eur. J.* **2018**, *24*, 4273–4278. [CrossRef]

82. Ji, L.; Li, L.; Ji, X.; Zhang, Y.; Mou, S.; Wu, T.; Liu, Q.; Li, B.; Zhu, X.; Luo, Y.; et al. Highly selective electrochemical reduction of CO_2 to alcohols on an FeP nanoarray. *Angew. Chem.* **2020**, *132*, 768–772. [CrossRef]

83. Guo, Y.; Wang, Q.; Wang, M.; Shen, M.; Zhang, L.; Shi, J. FeP modified polymeric carbon nitride as a noble-metal-free photocatalyst for efficient CO_2 reduction. *Catal. Commun.* **2021**, *156*, 106326. [CrossRef]

84. Ren, Y.; Li, Z.; Deng, B.; Ye, C.; Zhang, L.; Wang, Y.; Li, T.; Liu, Q.; Cui, G.; Asiri, A.M.; et al. Superior hydrogen evolution electrocatalysis enabled by CoP nanowire array on graphite felt. *Int. J. Hydrogen Energy* **2022**, *47*, 3580–3586. [CrossRef]

85. Jin, C.; Xu, C.; Chang, W.; Ma, X.; Hu, X.; Liu, E.; Fan, J. Bimetallic phosphide NiCoP anchored g-C3N4 nanosheets for efficient photocatalytic H_2 evolution. *J. Alloys Compd.* **2019**, *803*, 205–215. [CrossRef]

86. Gong, S.; Hou, M.; Niu, Y.; Teng, X.; Liu, X.; Xu, M.; Xu, C.; Au, V.K.M.; Chen, Z. Molybdenum phosphide coupled with highly dispersed nickel confined in porous carbon nanofibers for enhanced photocatalytic CO_2 reduction. *J. Chem. Eng.* **2022**, *427*, 131717. [CrossRef]

87. Zhu, J.; He, Q.; Liu, Y.; Key, J.; Nie, S.; Wu, M.; Shen, P.K. Three-dimensional, hetero-structured, $Cu_3P@C$ nanosheets with excellent cycling stability as Na-ion battery anode material. *J. Mater. Chem.* **2019**, *7*, 16999–17007. [CrossRef]

88. Hong, L.F.; Guo, R.T.; Yuan, Y.; Ji, X.Y.; Lin, Z.D.; Li, Z.S.; Pan, W.G. Recent progress of transition metal phosphides for photocatalytic hydrogen evolution. *ChemSusChem* **2021**, *14*, 539–557. [CrossRef] [PubMed]

89. Li, Y.H.; Qi, M.Y.; Li, J.Y.; Tang, Z.R.; Xu, Y.J. Noble metal free CdS@ CuS-NixP hybrid with modulated charge transfer for enhanced photocatalytic performance. *Appl. Catal. B* **2019**, *257*, 117934. [CrossRef]

90. Zou, Y.; Guo, C.; Cao, X.; Zhang, L.; Chen, T.; Guo, C.; Wang, J. Synthesis of CdS/CoP hollow nanocages with improved photocatalytic water splitting performance for hydrogen evolution. *J. Environ. Chem. Eng.* **2021**, *9*, 106270. [CrossRef]

91. Ray, A.; Sultana, S.; Paramanik, L.; Parida, K.M. Recent advances in phase, size, and morphology-oriented nanostructured nickel phosphide for overall water splitting. *J. Mater. Chem. A* **2020**, *8*, 19196–19245. [CrossRef]

92. Ali, S.A.; Ahmad, T. Enhanced hydrogen generation via overall water splitting using novel MoS_2-BN nanoflowers assembled TiO_2 ternary heterostructures. *Int. J. Hydrog. Energy* **2023**, *48*, 22044–22059. [CrossRef]

93. Zhang, X.; Yan, J.; Zheng, F.; Zhao, J.; Lee, L.Y.S. Designing charge transfer route at the interface between WP nanoparticle and $g-C_3N_4$ for highly enhanced photocatalytic CO_2 reduction reaction. *Appl. Catal. B* **2021**, *286*, 119879. [CrossRef]

94. Mehtab, A.; Banerjee, S.; Mao, Y.; Ahmad, T. Type-II $CuFe_2O_4$/graphitic carbon nitride heterojunctions for high-efficiency photocatalytic and electrocatalytic hydrogen generation. *ACS Appl. Mater. Interfaces* **2022**, *14*, 44317–44329. [CrossRef] [PubMed]

95. Shen, R.; Xie, J.; Ding, Y.; Liu, S.Y.; Adamski, A.; Chen, X.; Li, X. Carbon nanotube-supported Cu_3P as high-efficiency and low-cost cocatalysts for exceptional semiconductor-free photocatalytic H_2 evolution. *ACS Sustain. Chem. Eng.* **2018**, *7*, 3243–3250. [CrossRef]

96. Song, T.; Zhang, X.; Matras-Postolek, K.; Yang, P. N-doped carbon layer promoted charge separation/transfer in $WP/g-C_3N_4$ heterostructures for efficient H_2 evolution and 4-nitrophenol removal. *Carbon* **2023**, *202*, 378–388. [CrossRef]

97. Wang, F.; Qian, G.; Kong, X.P.; Zhao, X.; Hou, T.; Chen, L.; Fang, R.; Li, Y. Hierarchical double-shelled CoP nanocages for efficient visible-light-driven CO_2 reduction. *ACS Appl. Mater. Interfaces* **2021**, *13*, 45609–45618. [CrossRef] [PubMed]

98. Lv, X.; Li, X.; Yang, C.; Ding, X.; Zhang, Y.; Zheng, Y.Z.; Li, S.; Sun, X.; Tao, X. Large-size, porous, ultrathin NiCoP nanosheets for efficient electro/photocatalytic water splitting. *Adv. Funct. Mater.* **2020**, *30*, 1910830. [CrossRef]

99. Dou, M.Y.; Han, S.R.; Du, X.X.; Pang, D.H.; Li, L.L. Well-defined FeP/CdS heterostructure construction with the assistance of amine for the efficient H_2 evolution under visible light irradiation. *Int. J. Hydrogen Energy* **2020**, *45*, 32039–32049. [CrossRef]

100. Mishra, I.K.; Zhou, H.Q.; Sun, J.Y.; Qin, F.; Dahal, K.; Bao, J.M.; Chen, S.; Ren, Z.F. Hierarchical CoP/Ni$_5$P$_4$/CoP microsheet arrays as a robust pH-universal electrocatalyst for efficient hydrogen generation. *Energy Environ. Sci.* **2018**, *11*, 2246–2252. [CrossRef]
101. Tian, J.Q.; Liu, Q.; Asiri, A.M.; Sun, X.P. Self-supported nanoporous cobalt phosphide nanowire arrays: An efficient 3D hydrogen-evolving cathode over the wide range of pH 0-14. *J. Am. Chem. Soc.* **2014**, *136*, 7587–7590. [CrossRef]
102. Han, A.L.; Chen, H.L.; Zhang, H.Y.; Sun, Z.J.; Du, P.W. Ternary metal phosphide nanosheets as a highly efficient electrocatalyst for water reduction to hydrogen over a wide pH range from 0 to 14. *J. Mater. Chem. A* **2016**, *4*, 10195–10202. [CrossRef]
103. Li, J.; Zheng, H.; Xu, C.; Su, Z.; Li, X.; Sun, J. Bimetallic phosphides as high-efficient electrocatalysts for hydrogen generation. *Inorg. Chem.* **2021**, *60*, 1624–1630. [CrossRef]
104. Yang, M.; Jiang, Y.; Qu, M.; Qin, Y.; Wang, Y.; Shen, W.; He, R.; Su, W.; Li, M. Strong electronic couple engineering of transition metal phosphides-oxides heterostructures as multifunctional electrocatalyst for hydrogen production. *Appl. Catal. B Environ.* **2020**, *269*, 118803. [CrossRef]
105. Kang, Q.; Li, M.; Shi, J.; Lu, Q.; Gao, F. A universal strategy for carbon-supported transition metal phosphides as high-performance bifunctional electrocatalysts towards efficient overall water splitting. *ACS Appl. Mater. Interfaces* **2020**, *12*, 19447–19456. [CrossRef]
106. Chen, D.; Pu, Z.; Lu, R.; Ji, P.; Wang, P.; Zhu, J.; Lin, C.; Li, H.W.; Zhou, X.; Hu, Z.; et al. Ultralow Ru loading transition metal phosphides as high-efficient bifunctional electrocatalyst for a solar-to-hydrogen generation system. *Adv. Energy Mater.* **2020**, *10*, 2000814. [CrossRef]
107. Liu, Y.; Zhang, Z.; Zhang, L.; Xia, Y.; Wang, H.; Liu, H.; Ge, S.; Yu, J. Manipulating the d-band centers of transition metal phosphides through dual metal doping towards robust overall water splitting. *J. Mater. Chem. A* **2022**, *10*, 22125–22134. [CrossRef]
108. Zhang, H.; Aierke, A.; Zhou, Y.; Ni, Z.; Feng, L.; Chen, A.; Wågberg, T.; Hu, G. A High-performance transition-metal phosphide electrocatalyst for converting solar energy into hydrogen at 19.6% STH efficiency. *Carbon Energy* **2023**, *5*, 217. [CrossRef]
109. Pei, Y.; Cheng, Y.; Chen, J.; Smith, W.; Dong, P.; Ajayan, P.M.; Ye, M.; Shen, J. Recent developments of transition metal phosphides as catalysts in the energy conversion field. *J. Mater. Chem. A* **2018**, *6*, 23220–23243. [CrossRef]
110. Li, Y.; Dong, Z.; Jiao, L. Multifunctional Transition Metal-Based Phosphides in Energy-Related Electrocatalysis. *Adv. Energy Mater.* **2020**, *10*, 1902104. [CrossRef]
111. Downes, C.A.; Libretto, N.J.; Harman-Ware, A.E.; Happs, R.M.; Ruddy, D.A.; Baddour, F.G.; Ferrell III, J.R.; Habas, S.E.; Schaidle, J.A. Electrocatalytic CO$_2$ reduction over Cu$_3$P nanoparticles generated via a molecular precursor route. *ACS Appl. Energy Mater.* **2020**, *3*, 10435–10446. [CrossRef]
112. Sun, X.; Lu, L.; Zhu, Q.; Wu, C.; Yang, D.; Chen, C.; Han, B. MoP nanoparticles supported on indium-doped porous carbon: Outstanding catalysts for highly efficient CO$_2$ electroreduction. *Angew. Chem. Int. Ed. Eng.* **2018**, *57*, 2427–2431. [CrossRef]
113. Kim, M.G.; Choi, Y.; Park, E.; Cheon, C.H.; Kim, N.K.; Min, B.K.; Kim, W. Crystalline/Amorphous Ni$_2$P/Ho$_2$O$_3$ Core/Shell Nanoparticles for Electrochemical Reduction of CO$_2$ to Acetone. *ACS Appl. Energy Mater.* **2020**, *3*, 11516–11522. [CrossRef]
114. Laursen, A.B.; Calvinho, K.U.; Goetjen, T.A.; Yap, K.M.; Hwang, S.; Yang, H.; Garfunkel, E.; Dismukes, G.C. CO$_2$ electro-reduction on Cu$_3$P: Role of Cu (I) oxidation state and surface facet structure in C1-formate production and H$_2$ selectivity. *Electrochim. Acta* **2021**, *391*, 138889. [CrossRef]
115. Calvinho, K.U.; Alherz, A.W.; Yap, K.M.; Laursen, A.B.; Hwang, S.; Bare, Z.J.; Clifford, Z.; Musgrave, C.B.; Dismukes, G.C. Surface Hydrides on Fe$_2$P Electrocatalyst Reduce CO$_2$ at Low Overpotential: Steering Selectivity to Ethylene Glycol. *J. Am. Chem. Soc.* **2021**, *143*, 21275–21285. [CrossRef] [PubMed]
116. Banerjee, S.; Kakekhani, A.; Wexler, R.B.; Rappe, A.M. Mechanistic Insights into CO$_2$ Electroreduction on Ni$_2$P: Understanding Its Selectivity toward Multicarbon Products. *ACS Catal.* **2021**, *11*, 11706–11715. [CrossRef]
117. Rosser, T.E.; Windle, C.D.; Reisner, E. Electrocatalytic and Solar-Driven CO$_2$ Reduction to CO with a Molecular Manganese Catalyst Immobilized on Mesoporous TiO$_2$. *Angew. Chem. Int. Ed. Eng* **2016**, *55*, 7388–7392.
118. Liu, T.; Li, P.; Yao, N.; Cheng, G.Z.; Chen, S.L.; Luo, W.; Yin, Y.D. CoP-doped MOF-based electrocatalyst for pH-universal hydrogen evolution reaction. *Angew. Chem. Int. Ed.* **2019**, *58*, 4679–4684. [CrossRef]
119. Pan, Y.; Liu, Y.; Liu, C. Nanostructured nickel phosphide supported on carbon nanospheres: Synthesis and application as an efficient electrocatalyst for hydrogen evolution. *J. Power Sources* **2015**, *285*, 169–177. [CrossRef]
120. Niu, P.; Pan, Z.; Wang, S.; Wang, X. Cobalt Phosphide Cocatalysts Coated with Porous N-doped Carbon Layers for Photocatalytic CO$_2$ Reduction. *ChemCatChem* **2021**, *13*, 3581–3587. [CrossRef]
121. Zhang, Z.; Song, N.; Wang, J.; Liu, Y.; Dai, Z.; Nie, G. Polydopamine-derived carbon layer anchoring NiCo-P nanowire arrays for high-performance binder-free supercapacitor and electrocatalytic hydrogen evolution. *SusMat* **2022**, *2*, 646–657. [CrossRef]
122. Wang, J.; Liu, Z.; Zheng, Y.; Cui, L.; Yang, W.; Liu, J. Recent advances in cobalt phosphide-based materials for energy-related applications. *J. Mater. Chem. A* **2017**, *5*, 22913–22932.
123. Shah, S.S.A.; Khan, N.A.; Imran, M.; Rashid, M.; Tufail, M.K.; Rehman, A.U.; Balkourani, G.; Sohail, M.; Najam, T.; Tsiakaras, P. Recent Advances in Transition Metal Tellurides (TMTs) and Phosphides (TMPs) for Hydrogen Evolution Electrocatalysis. *Membranes* **2023**, *13*, 113. [CrossRef] [PubMed]
124. Zhao, H.; Yuan, Z.Y. Transition metal–phosphorus-based materials for electrocatalytic energy conversion reactions. *Catal. Sci. Technol.* **2017**, *7*, 330–347. [CrossRef]
125. Chu, Y.; Wang, D.; Shan, X.; Liu, C.; Wang, W.; Mitsuzaki, N.; Chen, Z. Activity engineering to transition metal phosphides as bifunctional electrocatalysts for efficient water-splitting. *Int. J. Hydrogen Energy* **2022**, *47*, 38983–39000. [CrossRef]

126. Du, H.; Kong, R.M.; Guo, X.; Qu, F.; Li, J. Recent progress in transition metal phosphides with enhanced electrocatalysis for hydrogen evolution. *Nanoscale* **2018**, *10*, 21617–21624. [CrossRef] [PubMed]

127. Zeng, D.; Xu, W.; Ong, W.J.; Xu, J.; Ren, H.; Chen, Y.; Zheng, H.; Peng, D.L. Toward noble-metal-free visible-light-driven photocatalytic hydrogen evolution: Monodisperse sub–15 nm Ni_2P nanoparticles anchored on porous g-C_3N_4 nanosheets to engineer 0D-2D heterojunction interfaces. *Appl. Catal. B* **2018**, *221*, 47–55. [CrossRef]

128. Zhang, R.; Wang, X.; Yu, S.; Wen, T.; Zhu, X.; Yang, F.; Sun, X.; Wang, X.; Hu, W. Ternary $NiCo_2P_x$ nanowires as pH-universal electrocatalysts for highly efficient hydrogen evolution reaction. *Adv. Mater.* **2017**, *29*, 1605502. [CrossRef] [PubMed]

129. Downes, C.A.; Van Allsburg, K.M.; Tacey, S.A.; Unocic, K.A.; Baddour, F.G.; Ruddy, D.A.; LiBretto, N.J.; O'Connor, M.M.; Farberow, C.A.; Schaidle, J.A.; et al. Controlled Synthesis of Transition Metal Phosphide Nanoparticles to Establish Composition-Dependent Trends in Electrocatalytic Activity. *Chem. Mater.* **2022**, *34*, 6255–6267. [CrossRef]

130. Irshad, S.; Ullah, F.; Khan, S.; Ludwig, R.; Mahmood, T.; Ayub, K. First row transition metals decorated boron phosphide nanoclusters as nonlinear optical materials with high thermodynamic stability and enhanced electronic properties; A detailed quantum chemical study. *Opt. Laser Technol.* **2021**, *134*, 106570. [CrossRef]